5-2021

Design, Construction, and Flight of a Remote-Controlled Aircraft for the 2020-21 AIAA DBF Competition

Jonathan A. Dixon
University of Tennessee, Knoxville, jdixon27@vols.utk.edu

Caleb Weatherly
University of Tennessee, Knoxville, cweath12@vols.utk.edu

Satyam Mistry
University of Tennessee, Knoxville, smistry@vols.utk.edu

Killian Samuels
University of Tennessee, Knoxville, ksamuel1@vols.utk.edu

Ethan Cerrito
University of Tennessee, Knoxville, ecerrito@vols.utk.edu

See next page for additional authors

Author

Jonathan A. Dixon, Caleb Weatherly, Satyam Mistry, Killian Samuels, Ethan Cerrito, Caleb Morgan, Sanghyeok Park, Sam Pankratz, and Jamison Murphree

THE UNIVERSITY OF TENNESSEE KNOXVILLE

The Spirit of Knoxville

List of Abbreviations and Symbols

AR	aspect ratio
a	lift curve slope (finite wing)
a_0	lift curve slope (semi-infinite wing)
a_t	lift curve slope (finite tail)
C_D	total Coefficient of Drag
C_{D0}	zero lift drag
$C_{D\text{-sensor}}$	coefficient of drag for the sensor
C_r	root chord
C_L	lift coefficient of wing
c_{mac}	mean aerodynamic chord length
C_t	tip chord
CFD	computational fluid dynamics
CG	center of gravity
D	drag on the airplane
EPP	Expanded Polypropylene
ESC	Electronic Speed Controller
F_D	force of drag
F_g	force of gravity
F_T	force of tension
FC	flight controller
h_n	distance from firewall to neutral point of the airplane (normalized by c_{mac})
h_l	distance from firewall to the aerodynamic center of the tail (normalized by c_{mac})
h_{nw}	distance from firewall to aerodynamic center of the wing (normalized by c_{mac})
K	lift-induced drag factor
L	force of lift
NP	neutral point
P	local pressure
S	reference area
S_t	planform area of the tail
T	local temperature
u_∞	freestream airspeed
VLM	Vortex Lattice Method
α	angle of attack
α_0	zero-lift angle of attack
$\Delta\%$	percent difference between predicted and actual values
ε_α	slope of downwash angle vs. angle of attack curve
η_t	tail efficiency factor
Λ_{LE}	sweep angle at the leading edge
$\Lambda_{0.25}$	sweep angle at the quarter chord
λ	taper ratio
ρ_∞	density of freestream air

I. Executive Summary

This report details the design, manufacture, and testing of the University of Tennessee's aircraft for the 2021 AIAA Design, Build, Fly competition. The competition features three missions: first, the airplane must be able to complete three laps around a predetermined course (Mission 1), carry as much cargo as possible and complete three laps as quickly as possible (Mission 2), and deploy and retract a towable sensor with functional lights, completing as many laps as possible in ten minutes (Mission 3). These mission requirements are at the core of the team's design, as the main goal of the competition is to maximize the score received for each of these missions.

Design Process

A sensitivity analysis of the impact of various design parameters on the total competition score was done to begin creating the preliminary model of the design. The propulsion system of the aircraft was designed first, as constraints to power, along with the need to stay in flight for a maximum of ten minutes, made the selection for this system relatively straightforward. Next, using the maximum power available from the propulsion system, along with the dimensions of the sensor and shipping containers, the dimensions for the fuselage were selected. Using flight test data from previous University of Tennessee DBF airplanes, the remaining components of the aircraft were designed. At the same time, the circuitry, fin structure, and deployment system for the sensor were designed and integrated into the overall aircraft design. The aircraft and sensor components were prototyped and tested to meet competition requirements and to maximize scoring parameters. After the testing phase, the final design was created and is documented in this report.

Selected Design and Key Parameters

The final design is a monoplane taildragger with a sensor deployment system integrated into the fuselage along with cargo space for simulated sensors. Key parameters for mission scoring are highlighted below in Table 1.1, along with the design performance and capabilities for these factors.

Table 1.1: Analysis of Scoring Parameters and Design Performance

Key Scoring Parameter	Design Performance
Maximum Takeoff Distance	~ 75 ft
Max Gross Weight	~ 20 lbs
Scorable Sensor Length	7 in.
Sensor Weight	8 oz.
Maximum Number of Sensors	9 shipping containers
Mission 2 Maximum Speed	122 ft/s
Estimated Laps in Mission 3	13
Estimated Ground Mission Time	180 s

Design Report Sections

The subsequent sections in this report highlight the team organization and schedule (**II. Management Summary**), the breakdown of scoring parameters and solutions to optimize total score (**III. Conceptual Design**), the methodology for design selection and predicting mission performance (**IV. Preliminary Design**), documentation of the final design (**V. Detail Design**), breakdown of component and design manufacturing (**VI. Manufacturing Plan**), description of testing and data collection (**VII. Testing Plan**), and performance of key subsystems and total design during testing (**VIII. Performance Results**).

II. Management Summary

Team Organization

The team was divided into sub-teams, but this structure was adjusted in response to changes in workload at different points in the design and construction phase. Due to the complexity of the sensor design, construction, testing, and integration, a sensor sub-team was created and maintained throughout the entire process. The remainder of the design and construction was divided into four sub-teams: Propulsion, Airframe, Computing, and Writing. The Propulsion Team was responsible for designing, testing, and assembling the propeller, motor, and related circuitry. The Airframe Team designed and built the structure of the aircraft (wings, fuselage, landing gear, and tail). The Computing Team made predictions of important features of aircraft performance. The Writing Team was established to ensure that the Proposal and Report were grammatically coherent and consistent. These latter two teams did not have responsibilities at all stages of the process, so members of these teams had other tasks on the other three teams as well. In January, the Propulsion and Airframe Teams were combined into a single team to ensure clear communication between them as the prototyping process neared completion. Both structures are shown in Fig 2.1.

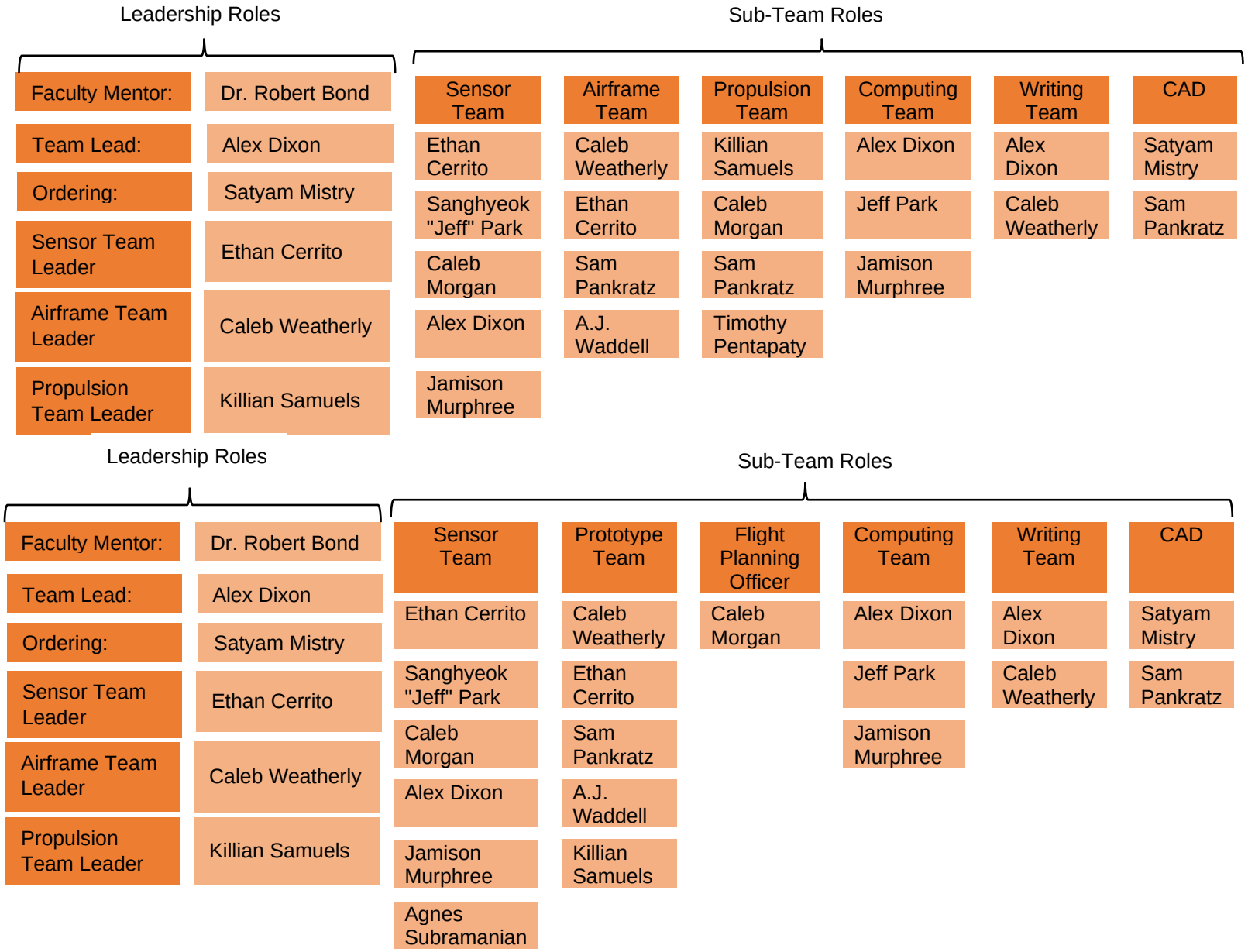

Figure 2.1: Chart of the initial (top) and final (bottom) division of labor.

Timeline

Due to the complexities of the COVID-19 pandemic, a flexible approach was taken to the team schedule. The initial timeline, created at the beginning of the design process, is given in Fig 2.2, and the adjusted timeline, which reflects the schedule changes made in response to the circumstances, is given in Fig 2.3.

Task Name	Duration	Start	Finish
Proposal	30 days	Mon 9/21/20	Sat 10/31/20
Rules and Mission Study	14 days	Mon 9/21/20	Thu 10/8/20
Organize Sub-teams	3 days	Thu 10/8/20	Mon 10/12/20
Conceptual Design	11 days	Thu 10/8/20	Thu 10/22/20
Preliminary Design	6 days	Fri 10/23/20	Fri 10/30/20
Proposal Due	0 days	Sat 10/31/20	Sat 10/31/20
Design Process	79 days	Mon 11/2/20	Fri 2/19/21
Prototype 1	41 days	Mon 11/2/20	Mon 12/28/20
Preliminary Design	4 days	Mon 11/2/20	Thu 11/5/20
Detailed Design	8 days	Fri 11/6/20	Tue 11/17/20
Construction	25 days	Wed 11/18/20	Tue 12/22/20
Flight Test	4 days	Wed 12/23/20	Mon 12/28/20
Prototype 2	38 days	Tue 12/29/20	Thu 2/18/21
Design Revision	6 days	Tue 12/29/20	Tue 1/5/21
Construction	20 days	Wed 1/6/21	Tue 2/2/21
Flight Test	5 days	Wed 2/3/21	Tue 2/9/21
Design Revision	8 days	Tue 2/9/21	Thu 2/18/21
Design Report Due	0 days	Fri 2/19/21	Fri 2/19/21
Final Design Process	36 days	Sat 2/20/21	Mon 4/12/21
Final Design Construction	29 days	Sat 2/20/21	Wed 3/31/21
Final Design Flight Test	5 days	Thu 4/1/21	Wed 4/7/21
Final Design Revision	3 days	Thu 4/8/21	Mon 4/12/21
Travel Days	2 days	Tue 4/13/21	Wed 4/14/21
AIAA Competition	4 days	Thu 4/15/21	Tue 4/20/21

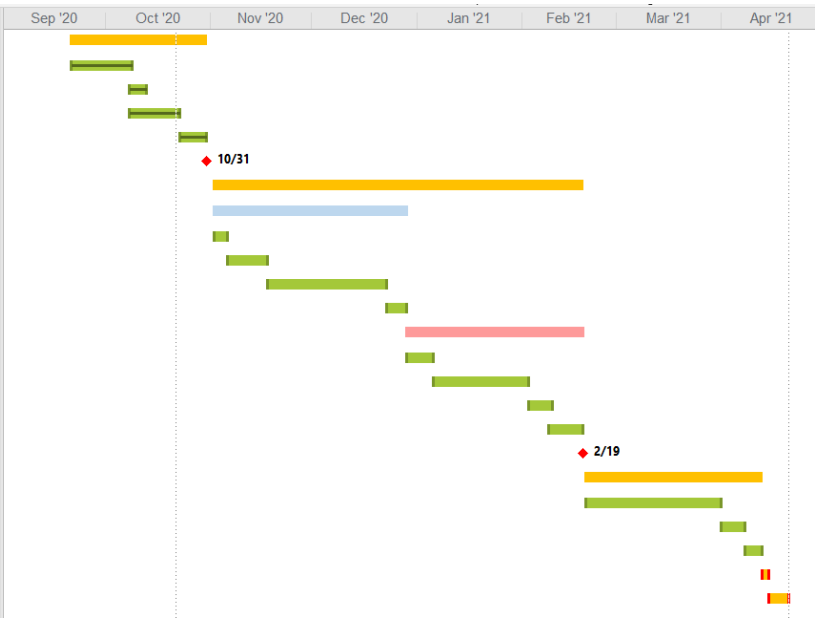

Figure 2.2: Initial Gantt chart

Task Name	Duration	Start	Finish
Proposal	30 days	Mon 9/21/20	Sat 10/31/20
Rules and Mission Study	14 days	Mon 9/21/20	Thu 10/8/20
Organize Sub-teams	3 days	Thu 10/8/20	Mon 10/12/20
Conceptual Design	11 days	Thu 10/8/20	Thu 10/22/20
Preliminary Design	6 days	Fri 10/23/20	Fri 10/30/20
Proposal Due	0 days	Sat 10/31/20	Sat 10/31/20
Design Process	75 days	Mon 11/2/20	Sun 2/14/21
Prototype 1	75 days	Mon 11/2/20	Sun 2/14/21
Preliminary Design	6 days	Mon 11/2/20	Sat 11/7/20
Detailed Design	7 days	Sun 11/8/20	Sat 11/14/20
Construction	17 days	Sun 11/22/20	Sat 12/12/20
Construction	15 days	Mon 1/11/21	Fri 1/29/21
Flight Test and Data Revision	12 days	Sat 1/30/21	Sun 2/14/21
Prototype 2	0 days	Sun 2/14/21	Sun 2/14/21
Design Revision			
Construction			
Flight Test			
Design Revision			
Design Report Writing	6 days	Sun 2/14/21	Fri 2/19/21
Design Report Due	0 days	Fri 2/19/21	Fri 2/19/21
Final Design Process	38 days	Sat 2/20/21	Wed 4/14/21
Final Design Construction	29 days	Sat 2/20/21	Wed 3/31/21
Final Design Flight Test	5 days	Thu 4/1/21	Wed 4/7/21
Final Design Revision	5 days	Thu 4/8/21	Wed 4/14/21
AIAA Competition	4 days	Thu 4/15/21	Tue 4/20/21

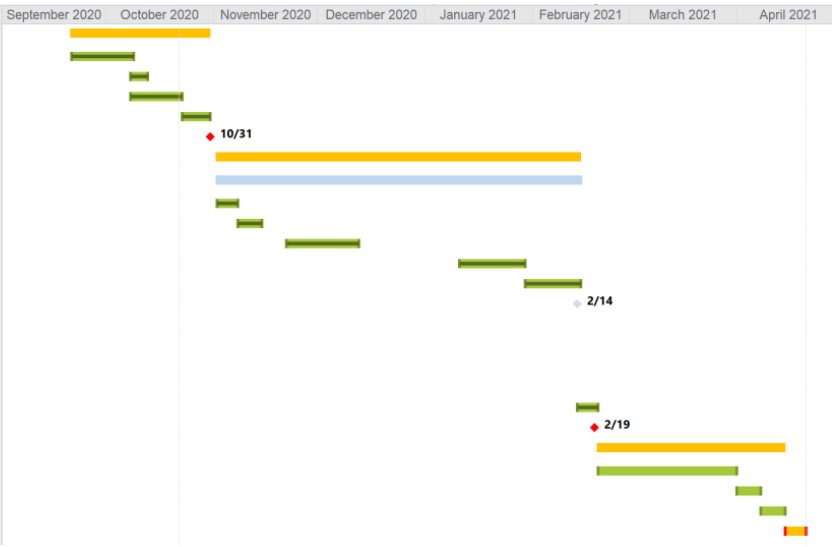

Figure 2.3: Final Gantt chart

Due to COVID-19 changes, the university was closed for winter break from November 24, 2020 to January 20, 2021, so little work was accomplished during this time. Considering this constraint, the team decided that it would be more useful to focus on the design, manufacture, and testing of a single prototype than to rush through the design, manufacture, and testing of two prototypes. The latter option would risk poor performance on both prototypes, making the process for the final airplane more difficult. By restricting its focus to a single prototype, the team was able to make useful progress toward a design that would perform each of the four missions well.

III. Conceptual Design

The team's conceptual approach to the Design, Build, Fly Competition has remained unchanged since the Proposal phase.

Problem Statement

The 2021 Design, Build, Fly Competition is divided into four missions (three flight missions and one ground mission). The specific requirements are summarized in Table 3.1.

Table 3.1: Mission Requirements [1]

Mission	Requirements
Ground Mission	**1.** Perform drop test of shipping container **2.** Load and unload Mission 2 payload (all shipping containers and deployment system) **3.** Deployment and recovery of sensor
Mission 1	**1.** Take off in under 100 ft and land successfully **2.** Complete three laps in under 5 minutes
Mission 2	**1.** Take off in under 100 ft and land successfully **2.** Carry a maximum number of shipping containers and deployment system **3.** Complete three laps
Mission 3	**1.** Take off in under 100 ft and land successfully **2.** Carry, deploy, and recover one aerodynamically stable sensor **3.** Operate sensor lights one at a time **4.** Complete as many laps as possible in ten minutes

Subsystem Design Requirements

The above requirements were translated into requirements for each sub-team (Sensor, Airframe, and Propulsion), described in Table 3.2.

Table 3.2: Sub-System Requirements		
Subteam	**Subsystem**	**Requirement**
Sensor	Circuitry	**1.** Be as compact as possible. **2.** Include lights that can easily be viewed from the ground when the airplane is at the opposite end of the course. **3.** Include batteries capable of powering the lights. **4.** Accept input from the radio receiver so that the lights can be turned on and off by the radio transmitter.
	Structure (nosecone, body, and fins)	**1.** Maintain aerodynamic stability during deployment, cruise, and retraction. **2.** Provide structure for the circuitry without obscuring the lights.
	Shipping container	**1.** Be strong enough to protect the sensor from damage when dropped from 10 inches. **2.** Be strong enough to sustain only cosmetic damage when dropped from 10 inches. **3.** Minimize weight.
	Deployment Mechanism	**1.** Deploy and retract the tow cable and signal wire for the sensor. **2.** Present minimal additional drag during sensor deployment and retraction. **3.** All servo operations must be controlled by the radio transmitter.
Airframe	Wings	**1.** Generate sufficient lift to support the estimated weight of the airplane. **2.** Minimize induced drag. **3.** Minimize short-coupling.
	Horizontal Stabilizer	**1.** Be large enough to ensure stability and control for takeoff and cruise.
	Vertical Stabilizer	**1.** Be large enough to provide yaw stability.
	Landing Gear	**1.** Mount onto the fuselage at an angle relative to the ground that would transmit the shock of landing to the fuselage without shearing off. **2.** Be large enough to allow sufficient ground clearance for the intended range of propeller sizes (18” – 20” diameter).
	Fuselage	**1.** Be strong enough to support its own weight. **2.** Spread the force of lift (from the wing spar) to the rest of the airframe. **3.** Minimize weight. **4.** Spread the force of landing (from the landing gear) to the rest of the airframe. **5.** Contain and provide easy access to the electrical components (e.g. the main batteries).
Propulsion	Propeller	**1.** Transmit power at peak propeller efficiency at the estimated cruise speed for each mission.
	Motor	**1.** Provide maximum power for propulsion without excessive battery consumption (i.e., must consume battery power at a rate that permits the successful completion of each mission).
	ESC	**1.** Be rated to handle the voltage and current delivered to the motor.
	Main batteries	**1.** Contain a high power-to-weight ratio. **2.** Contain the maximum allowable amount of energy (100 watt-hours per battery).
	Servos	**1.** Be strong enough to manipulate their respective control surfaces. **2.** Manipulate their respective control surfaces with precision.

Scoring Sensitivity Analysis

Before designing the airplane, the team developed a MATLAB® program to determine the contribution of certain features of the airplane's design to its overall competition score. This program was designed to consider four variables: airspeed, sensor length, sensor weight, and the quantity of sensors. The impact of each variable on the total score was calculated by holding the other three constant and testing values of the independent variable. The results of this analysis are shown in Fig. 3.1. A loss of sensor weight decreased the score the least, and an increase in the sensor length increased the score the most, so the team decided to design the airplane to maximize sensor length and minimize sensor weight.

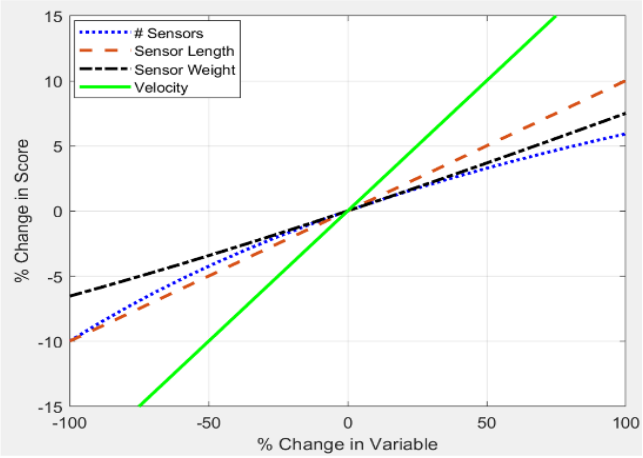

Figure 3.1: The results of the team's sensitivity study [1]

Configurations Considered

The team took a component-based approach to design, so possible configurations were considered by evaluating the options for each subsystem. Table 3.3 summarizes these options, which were also presented in the Proposal.

Table 3.3: Configurations Considered by Subsystem				
Subsystem	**Component**	**Options Considered**		
		Option 1	**Option 2**	**Option 3**
Propulsion	Number of Engines	One	Two	
	Direction of Propeller	Tractor		
	Location of Engines	Centerline (nose)	Wings	
Sensor	Shipping Container Material	PVC	Cardboard	
	Shipping Container Shape	Cylindrical	Rectangular Prism	Triangular Prism
	Deployment Mechanism	Bomb bay structure (two-door)	Bomb bay structure (single door)	
	Fins	Conformal	Externally mounted	
Airframe	Fuselage Material	Balsa wood	Lite Plywood	Composite
	Fuselage Cross-sectional Shape	Square	Circle	Triangle
	Shape of Wing Planform	Delta (Flying Wing)	Straight, untapered	Straight, tapered
	Airfoil Section	NACA 2408	NACA 2410	NACA 23012
	Landing Gear Configuration	Tail dragger	Tricycle	

Selection of Final Configuration

Narrowing the list of options for each component was a crucial stage that defined the trajectory of the rest of the design process, so these selections were made with input from the entire team. Options were organized into a collaborative Google Sheets document, allowing every team member to review the various configurations and to discuss them in our virtual meetings. To select the final configuration for each component, the team adopted a design philosophy of simplicity over complexity and drew on the knowledge and experiences of each team member. The final concept for each component and the rationale behind its selection is given in Table 3.4.

Table 3.4: Final Concept for Each Component			
Subsystem	**Component**	**Final Concept**	**Rationale**
Propulsion	Number of Engines	One	Requirements for multiple propellers (extra battery weight, etc.) would outweigh the benefit of added thrust. Also, there was risk of yaw instability from out-of-sync engines.
	Direction of Propeller	Tractor	No significant benefit was anticipated from using a pusher over a tractor, so the traditional structure was selected.
	Location of Engines	Centerline	Any other location would require input from one or more control surfaces, needlessly increasing the induced drag.
Sensor	Shipping Container Material	Cardboard	This was determined after tests of the sensor circuitry. The size of the sensor was too large for a thin-schedule PVC pipe.
	Shipping Container Shape	Rectangular prism	The Q&A #1 document restricted the options to a rectangular prism and a cylinder, and for ease of construction, a rectangular prism was selected.
	Deployment Mechanism	Bomb bay structure	Including doors that open only when the sensor is passing into or out of the fuselage would create less parasitic drag than the single-door approach would, since this approach would require that the door hang below the fuselage until the sensor is retracted (i.e., in order not to interfere with the tow cable).
	Fins	Externally mounted	Aerodynamic testing (Section VIII 2B) suggested this configuration was more stable than the conformal option.
Airframe	Fuselage Material	Balsa wood	The team's inexperience with composites and the weakness of foam relative to the target airspeed left balsa wood as the most viable option.
	Fuselage Cross-sectional Shape	Square	Efficient use of internal storage space and ease of construction pointed to a square cross-section.
	Shape of Wing Planform	Straight, tapered	Simplicity pointed to a non-delta wing and the minimization of induced drag indicated a taper ratio as close to 0.3 as possible (at the recommendation of our faculty advisor).
	Airfoil Section	NACA 2408	The NACA 4-Series was chosen for ease of manufacturing, and the thinnest airfoil that would provide sufficient lift was selected in order to minimize drag.
	Landing Gear Configuration	Tail dragger	Experience from an RC pilot suggested this would be more stable on the ground than a tricycle configuration.

IV. Preliminary Design

The preliminary design of each component was developed in response to the question, "what features should this system have in order to maximize the overall score?" With input from an experienced RC pilot, each parameter was maximized within reason to create the estimated highest-scoring preliminary design possible. The preliminary design for each component is described below, along with the reasoning behind each design.

A. Fuselage

- Structural Integrity – The preliminary design for the fuselage was adapted from data from previous flights conducted by University of Tennessee teams. The current design used this previous prototype's wing spar system, motor mount design, and tail structure, as they had performed well in both ground and flight testing on the prototype. However, the landing gear mounting was redesigned, as flight testing conducted by this previous University of Tennessee team highlighted this region of the fuselage as a weak point.
- Payload Requirements – Knowing the weight of each shipping container and the maximum gross weight that the propulsion system could support before failing to provide the thrust needed for takeoff, the fuselage was designed to fit as many shipping containers as possible.. Components for the deployment and recovery of the sensor were also added to the design for Mission 3 requirements.
- Weight/Drag Reduction – The preliminary design of the fuselage also focused on reducing weight and drag wherever possible. This meant minimizing the cross-sectional area of the fuselage wherever possible and minimizing the weight of the structure so that more weight could be dedicated to the payload. To minimize the cross-sectional area, the fuselage height and width were decreased to fit the payload as tightly as seemed reasonable, and the non-cargo regions were tapered. Reducing drag increases the design's maximum flight speed, therefore increasing score on Missions 2 and 3. The weight was reduced primarily through the material selection for the fuselage, as well as minimizing the total length of the fuselage.

B. Landing Gear

- Design Selection – The tail-dragger configuration was chosen because it allowed a higher angle of attack on takeoff, which allowed for more weight in the aircraft while still meeting takeoff length requirements. It was also more structurally stable on landing, allowing the design to better meet the requirement of a successful landing.

Weight Reduction – Weight was minimized in the landing gear by using a 3D-printed infusion mold, minimizing the amount of carbon fiber support present in the design. After infusion, the part was also sanded and non-load bearing portions of the component were trimmed away.

C. Wing/Tail

- Aspect Ratio – In general, high aspect ratio wings reduce the induced drag of an aircraft, allowing for a more efficient performance. However, the total wingspan of the competition design is limited to 5 feet, so the preliminary wing was designed with this maximum allowable wingspan, while wing area was minimized (using the results of wing load testing, performed on the prototype model) to maximize aspect ratio and thus increase the performance of the overall design, thus increasing the score for Missions 2 and 3.

- Wing Area – Using results from prototype flight testing as well as an estimated maximum allowable weight from propulsion system modeling and testing, the wing was designed with a total area of 7 ft^2, giving the complete design an estimated wing loading of 45 oz/ft^2 during Mission 2, in which the aircraft will be its heaviest. This ensures structural stability of the design while maximizing the in-flight performance, and thus the scoring, of the design.
- Airfoil – Since a relatively large wing area was selected for the design of the aircraft, the thickness of the airfoil was minimized to reduce the overall weight of the wing as well as the profile drag produced by the wing. A NACA 2408, 2410, and 23012 were considered. The NACA 2408 airfoil was selected for its reduced thickness and ease of manufacturing. Since the lift to drag curves for all three airfoils were similar, small imperfections in manufacturing would negate any minor performance advantages any of the three airfoils have.
- Tail Volume – Horizontal and vertical stabilizer sizing was based on predetermined wing area and fuselage length. Initial flight tests of the prototype revealed inertial coupling in the current design, so horizontal stabilizer area was reduced in order to achieve more stable flight characteristics of the final design. Values for desired tail volume coefficients were taken from historical data [8], which were then used to create dimensions of the horizontal and vertical stabilizers, along with input from an experienced RC pilot and the faculty advisor.

D. Propulsion

The propulsion system was designed to attain maximum performance for a duration of up to 10 minutes, while conserving weight and space within the airplane. The initial decision for the propulsion system was a single brushless motor operated by lithium polymer (LiPo) batteries with a 2-blade propeller.

Based on time predictions for each mission and the power constraints of 200 W-h, two 8S Thunder Power RC ELITE Series LiPo 3300mA-h batteries were connected via parallel circuit. This doubles the capacity to 6600mA-h while maintaining a continuous voltage of 29.6V. This allows for a total battery capacity of 195.36 Watt-hours to be supplied to the brushless motor. To accommodate for this amount of power, the MOTROLFLY DM-5320 330KV brushless motor was chosen for all missions. This motor is rated for 8S LiPo batteries with a max power of 2700W. The Phoenix Edge HV 120 electronic speed controller was selected because of its maximum current capability of 120 A, which exceeds the allowable current for the motor (91.22 A) and thus prevents overheating.

The optimal diameter of the propeller for the chosen brushless motor is between 18 and 19 inches. MATLAB was used to estimate the ideal pitch of a 2-blade propeller that would supply the best performance for the estimated parameters. Using an ideal mechanical efficiency of 80% and calibrating the batteries' current output to allow for the predicted flight time, along with other structural parameters of the aircraft, ideal cruise airspeeds were found. These airspeeds were expressed as advance ratio, which was then evaluated on a fixed pitch diagram to find the ideal pitch with respect to a chosen diameter. These data points were curve-fit to develop Figure 4.1, which was used to choose the optimal sizing. These calculations determined that a 19"x10" propeller will produce the ideal performance required for all three missions.

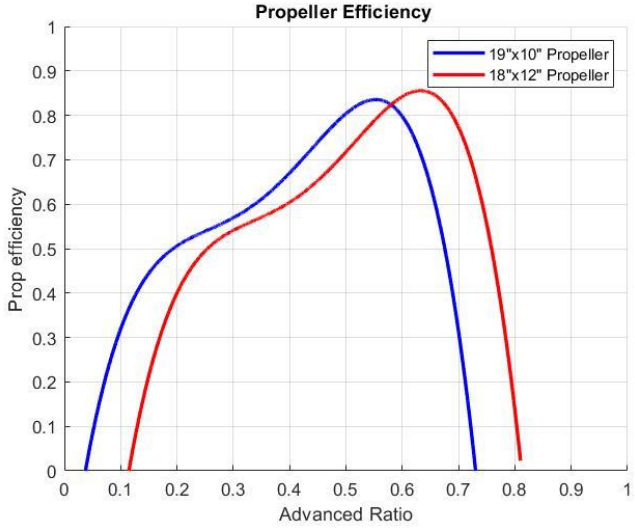

Figure 4.1: Propeller Efficiency versus Advance Ratio (J)

E. Sensor

- Deployment System – The "deployment mechanism" refers to the components necessary for storing, deploying, and retracting the sensor. This structure was intended to be a self-contained box that could easily be integrated into the fuselage. The least-complex version of this device still required several parts to fit together with tight tolerances, which indicated that it would be helpful to keep the systems in a single box rather than trying to match up hole positions, servo holders, etc. in the design of the fuselage itself. In addition to holding the sensor and connecting it to the radio receiver in the aircraft during Mission 3, the deployment mechanism was also designed to hold the sensor in its shipping container during Mission 2. Designing the cargo bay to hold a shipping container, rather than just the sensor itself, prevented the cargo bay from being empty space during Mission 2.

  The deployment mechanism is winch-based, using a continuous servo to control the direction of rotation. A slip ring allows the electrical signal from the radio receiver to be transmitted to the Arduino microcontroller inside the sensor. At the bottom of the mechanism are two doors, hinged on opposite sides of the centerline of the fuselage. Both are attached to mechanically independent servos.

- Sensor Structure and Stability – Aerodynamic structures with known aerodynamic stability, e.g. rockets and missiles, typically feature a rounded nose cone, long cylindrical body, and a finned tail section, so these features were chosen for the preliminary design of the sensor. Various nose cones and tail fin structures were designed in Onshape so that aerodynamic testing could be conducted to determine the best combination of stability, weight, and size. Two nose cone shapes were chosen for testing: a half-sphere and a half prolate spheroid. Four tail cone geometries, shown in Figure 4.2, were also selected: (1) conformal, full-length-of-tail fins; (2) conformal stub fins; (3) conformal stub fins with a ring; and (4) external fins. In this context, "conformal" indicates fins that do not extend past the maximum diameter of the sensor body itself, and "external" indicates fins that did extend past the maximum sensor diameter. After testing, it was found that the external fin design was the most stable in flight, so it was chosen for the final design of the sensor. It was also decided to minimize sensor diameter as much as possible while still allowing room for the electronics package to fit within the

sensor body. This decision was made to reduce individual sensor weight, and thus increase the number of sensors that could be carried by the aircraft.

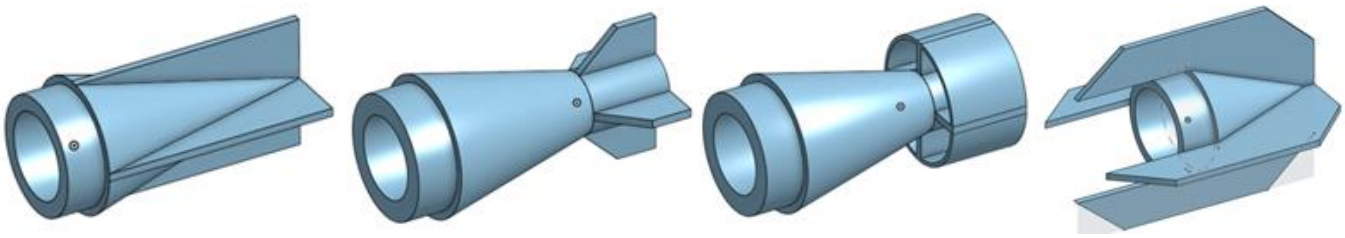

Figure 4.2: From left to right, tail designs 1-4.

- Circuitry – The final circuit consisted of one ELEGOO Nano microcontroller, three BC 547 transistors, three 220-ohm resistors, two 9-volt batteries, and three Chanzon RGB High Power LEDs. The microcontroller was connected to a receiver (FrSky X8R with SBUS). These parts were chosen based on the size limitation of the inner diameter of the cylindrical cardboard sensor fuselage. Fig. 4.3 shows a complete circuit diagram. The wire from D5 is the signal input from the receiver, the 5V pin connects to the positive polar, and the GND pin connects to the negative polar.

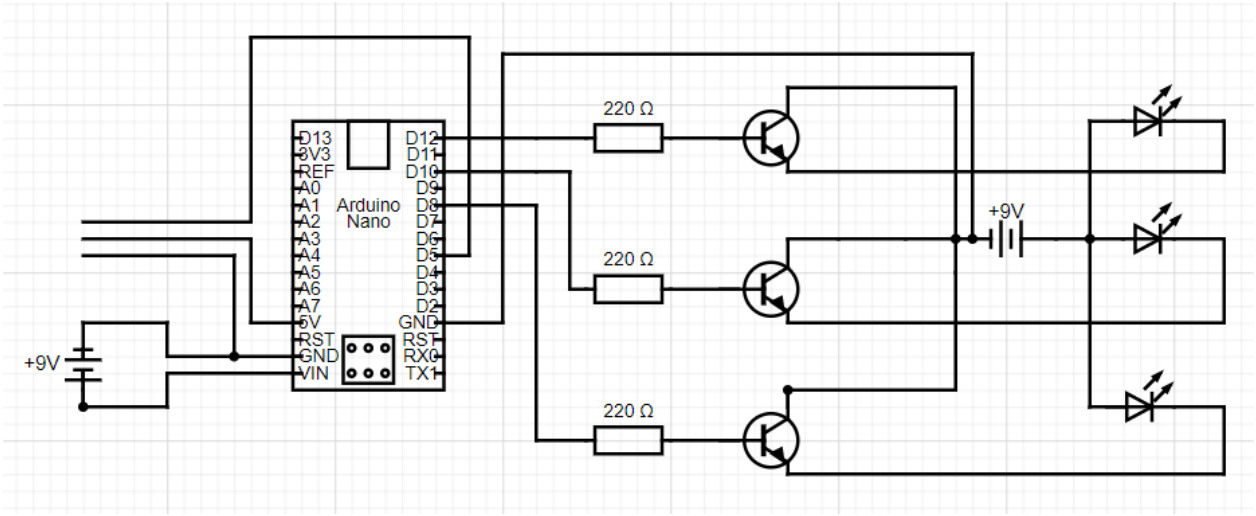

Figure 4.3: Circuit Diagram

- Cargo Container -- The main limitation of the cargo capacity of the aircraft was weight. The aircraft was expected to be able to support and effectively fly with a maximum total weight of twenty pounds. The aircraft weighed approximately twelve pounds, which left eight pounds of available cargo capacity. Therefore, the goal was to keep the weight of each sensor container to a minimum in order to maximize the number of simulated sensors that could be stored in the aircraft. The container was constructed out of cardboard in a 3”x3”x12” rectangular prism. Packing paper was placed on both ends of the sensor when it was loaded into the container to absorb impact from the drop test. The simulated sensor container shape and dimensions are identical to the actual sensor container, per competition guidelines. The only difference was that the simulated sensors were weighted with plastic bags filled with lead shot.

F. Drag Analysis

To estimate the drag of the aircraft in its three mission configurations the drag polar equation (Eq. 1) was used:

$$C_D = C_{D0} + KC_L^2 \ (+C_{D\text{-sensor}}), \quad \text{where} \quad D = \frac{1}{2}\rho_\infty {u_\infty}^2 S C_D \tag{1}$$

The drag polar of the aircraft was broken down into its two components(zero-lift drag and induced drag) in order to perform a drag analysis of the design. The zero-lift drag was estimated to be the total wetted surface area of the aircraft multiplied by an equivalent skin friction coefficient of 0.025, which was estimated from flight test data. The lift-induced drag of the aircraft was estimated as a function of wing geometry, airspeed, and weight of the aircraft, assuming steady, level flight for a majority of the flight time of each mission. For mission three, the drag force acting on the deployed sensor was estimated from flight test data, and this value was used to estimate the coefficient of drag for the sensor. These values were then calculated for varying airspeeds, and the results of the drag analysis are shown below in Figure 4.4. At higher velocities, the main component of drag is the parasitic drag, so the wetted surface area was reduced as much as possible, primarily through ensuring a smooth finish on all exterior surfaces. Mission 1 was not analyzed, since the full points for the mission are awarded for the completion of three laps, regardless of the speed of the aircraft.

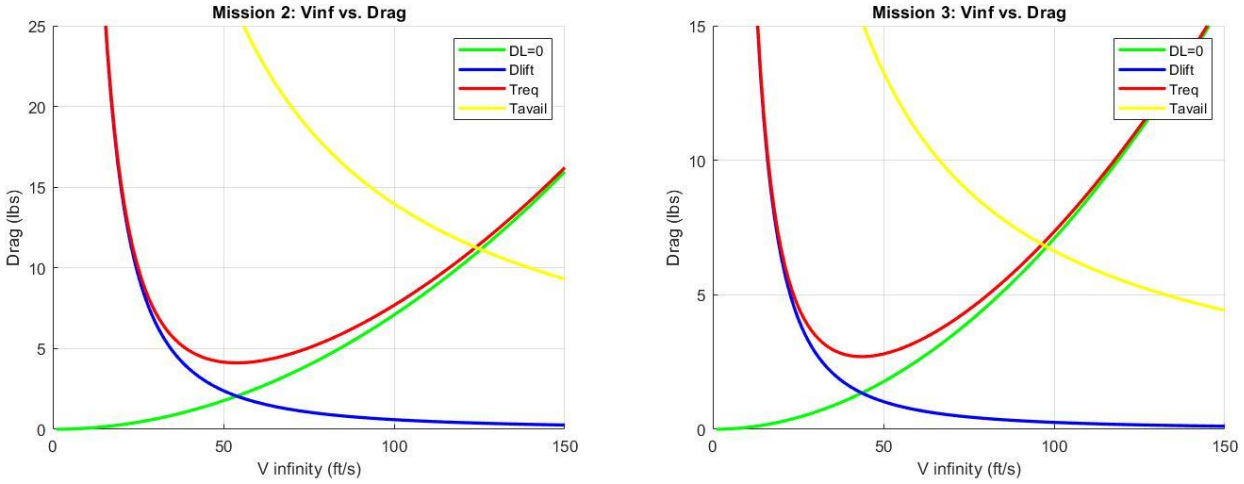

Figure 4.4: Drag Analysis for Mission 2 (left) and Mission 3 (right). The green line is the zero-lift drag, the blue line is the lift-induced drag, the black line is the drag of the deployed sensor (only for Mission 3), the red line is the thrust required to maintain the current velocity (i.e., the summation of all drag terms), and the yellow line is an estimate of thrust available from the propulsion system.

G. Lift Analysis

To estimate the lift that would act on the competition airplane, the basic lift equation was used (Eq. 2)

$$L = \frac{1}{2}\rho_\infty {u_\infty}^2 S C_L \tag{2}$$

where ρ_∞ (taken as 0.002329 slug/ft^3, accounting for local weather and altitude) and S (7 ft^2) were known constants and u_∞ adopted one of several known values (i.e., one of the cruise speeds presented in Table 4.1). The challenge, however, was to determine the lift coefficient of the wing, C_L. The value of the lift coefficient varied with angle of attack, so to classify the lift over the wing properly, an equation for the lift coefficient versus angle of attack was needed, in the form of Eq. 3:

$$C_L = a(\alpha - \alpha_0) \tag{3}$$

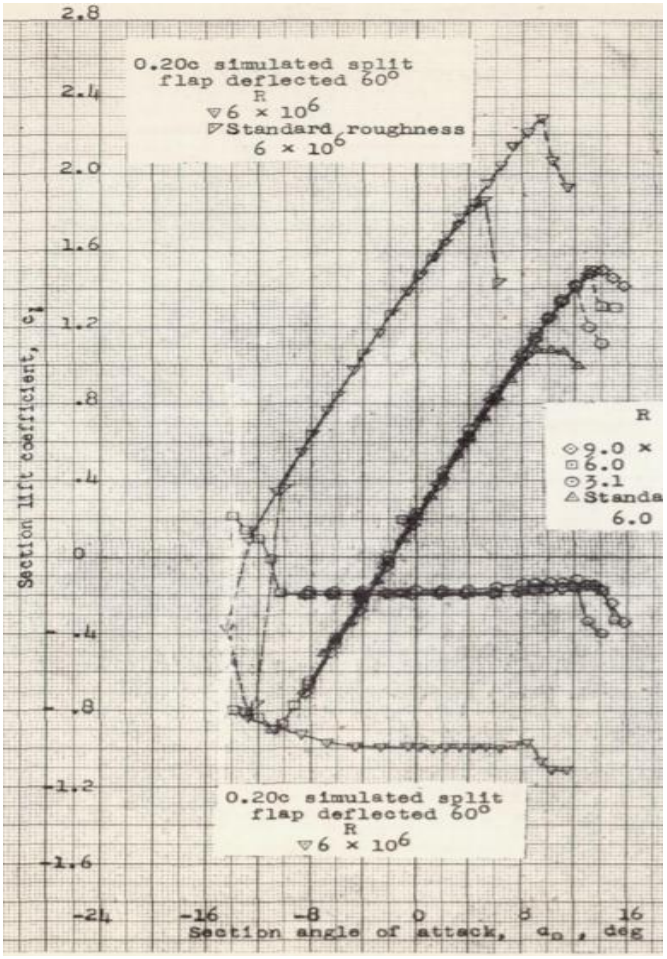

Figure 4.5: Original NACA 2408 test data [3]

To make this determination, NACA data for the lift coefficient versus angle of attack for the NACA 2408 airfoil section (i.e., the semi-infinite airfoil) was used (Fig. 4.5). These data were extended to the case of the finite wing through the Vortex Lattice Method, which was implemented in MATLAB.

This script accepted as inputs the various geometric parameters of the wing (AR, λ, and $\Lambda_{0.25}$) and the zero-lift angle of attack (from the NACA lift coefficient data). The script used these parameters to calculate the impact of wingtip vortices on the lift coefficient, yielding the slope of the lift coefficient vs. angle of attack for the wing.

Using the properties of the wing (AR = 3.57, λ = 0.591, and $\Lambda_{0.25}$ = 10.4625°) and the NACA 2408 (a_0 = 5.9086 1/rad; estimated from the plot in Fig. 4.5), the lift curve slope of the wing was calculated to be a = 3.6843 1/rad. Estimating α_0 = -2° (0.034907 rad) from the NACA data allows Eq. 2 to be defined in terms of angle of attack (Eq. 4):

$$L = \frac{1}{2}\rho_\infty {u_\infty}^2 S\big(a(\alpha - \alpha_0)\big) \qquad (4)$$

where $\alpha \in (-10°, 10°)$ (to avoid flow separation). This equation has been evaluated for takeoff and cruise for each flight mission.

Table 4.1 illustrates the range of lift performance expected for the competition plane. If the airplane were to fly at its maximum lift coefficient, it would generate as much as 95 lb of lift at its intended cruising airspeed. By flying between a 0° angle of attack and a 10° angle of attack, the competition plane will be able to generate enough lift to balance its weight for each mission configuration.

Table 4.1: Lift Force for Each Flight Regime

Regime	Airspeed (ft/s)	Min Angle of Attack (deg)	Max Angle of Attack (deg)	Lift Force (lb) at Min Angle of Attack	Lift Force (lb) at Max Angle of Attack
Cruise, Mission 1	123	0	10	15.86	95.16
Cruise, Mission 2	122	0	10	15.60	93.62
Cruise, Mission 3	87	0	10	6.767	40.60

H. Stability Characteristics

To determine the stability of the airplane, the slope of its pitching moment-angle of attack plot (Fig. 4.6) was calculated; a negative slope would indicate that the airplane would remain stable. The slope of the moment about the center of gravity with respect to the angle of attack was calculated to be -0.03615, indicating that the airplane would be stable.. A summary

of parameters affecting design stability is shown in Table 4.2. The center of gravity in every mission is in front of the neutral point, indicating that the airplane is stable for all missions.

Table 4.2: Design Parameters Affecting Stability	
Parameter	**Distance from Firewall**
LE of wing	13.46 in.
AC of wing	18.51 in.
AC of horizontal stabilizer	51.88 in.
Neutral Point of Plane	25.13 in.

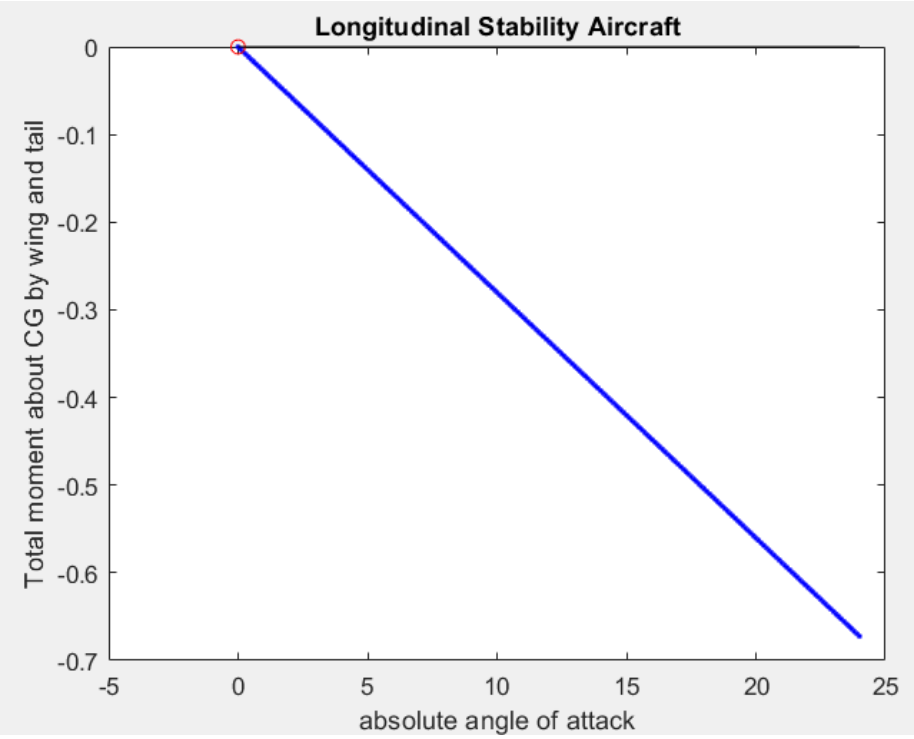

Figure 4.6: Stability Analysis for Design

I. Prediction of Sensor Stability

The initial concepts for sensor design resembled rockets, so the initial plan was to use rocket-based software to predict aerodynamic stability. However, these efforts were unsuccessful, due to software restrictions and the steep learning curve associated with CFD software. To make up for this, a variety of sensor fin structures were designed and manufactured so that aerodynamic testing would be able to identify a successful design.

It was also noted that the sensor designs resembled ordinances dropped by bombers during the Second World War. Since footage exists of these bombs being released, this was used to estimate the stability of a similarly-shaped atmospheric sensor. It seemed that the conformal fin structure was aerodynamically stable when deployed, so it was estimated that this design would work well in our application [5].

J. Mission Performance

The performance of each mission was evaluated under the assumption that the current drawn from the battery was constant. Using the power available for each mission, the takeoff acceleration was calculated to determine the duration of the takeoff stage of each mission. By using a set interval of velocities, before reaching the max cruise speed, the acceleration is interpreted (see Figure 4.7) to find the distance and time expended until a constant velocity is maintained. For simplicity of the analysis, the cruise velocity is assumed to remain constant for the remaining portion of the flight in each mission.

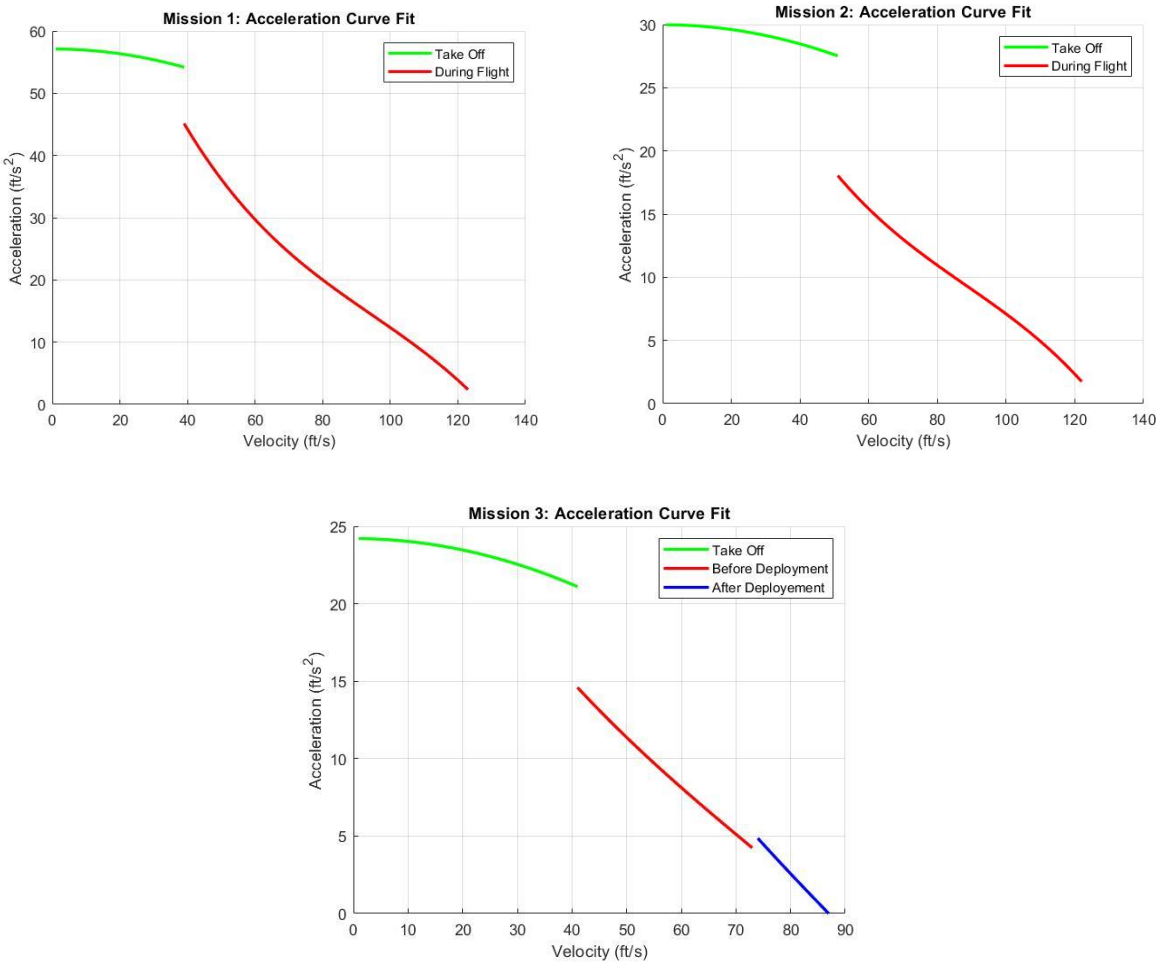

Figure 4.7: Acceleration Curve Fits for Mission 1, 2, and 3 (Left, Right, and Bottom)

Using estimated maximum flight times for the missions, a target current draw from the battery was determined for each case. For Missions 1 and 2, a maximum flight time of 5 minutes is approximated, while the allowed 10 minutes is used for the third. Comparing these times to the total battery capacity of 6600 mA-h, a continuous amperage was found. The maximum power constraints of the motor and electronic speed controller , along with a safety factor for the battery capacity, are factored into the target current draw. Table 4.3 and Figure 4.8 describe how this current draw, aircraft weight, and propeller efficiency affect the estimated max cruise velocity. In Figure 4.8, the red lines represent the power available with respect to the efficiency of the chosen propeller, the blue lines represent the power available assuming a constant propeller efficiency, and the green line displays the estimated required power at a given flight speed. These data were based on an estimate for the average temperature and density of Knoxville in April, where the design will be conducting its competition flights. Data in both Table 4.3 and Figure 4.8 will be tested and confirmed, as described in the Testing Plan section of the report.

Table 4.3: Propulsion System Parameters and Performance						
	Ideal Current Input	**Aircraft Weight (lbs)**	**Propeller Size**	**Static Thrust (lbf)**	**Max Velocity (ft/s)**	**Max Velocity (mph)**
Mission 1	80 Amps	14.00	19”x10”	25.68	123.0	83.86
Mission 2	80 Amps	18.34	19”x10”	27.07	122.0	83.18
Mission 3	38 Amps	14.63	19”x10”	12.51	87.00	59.32

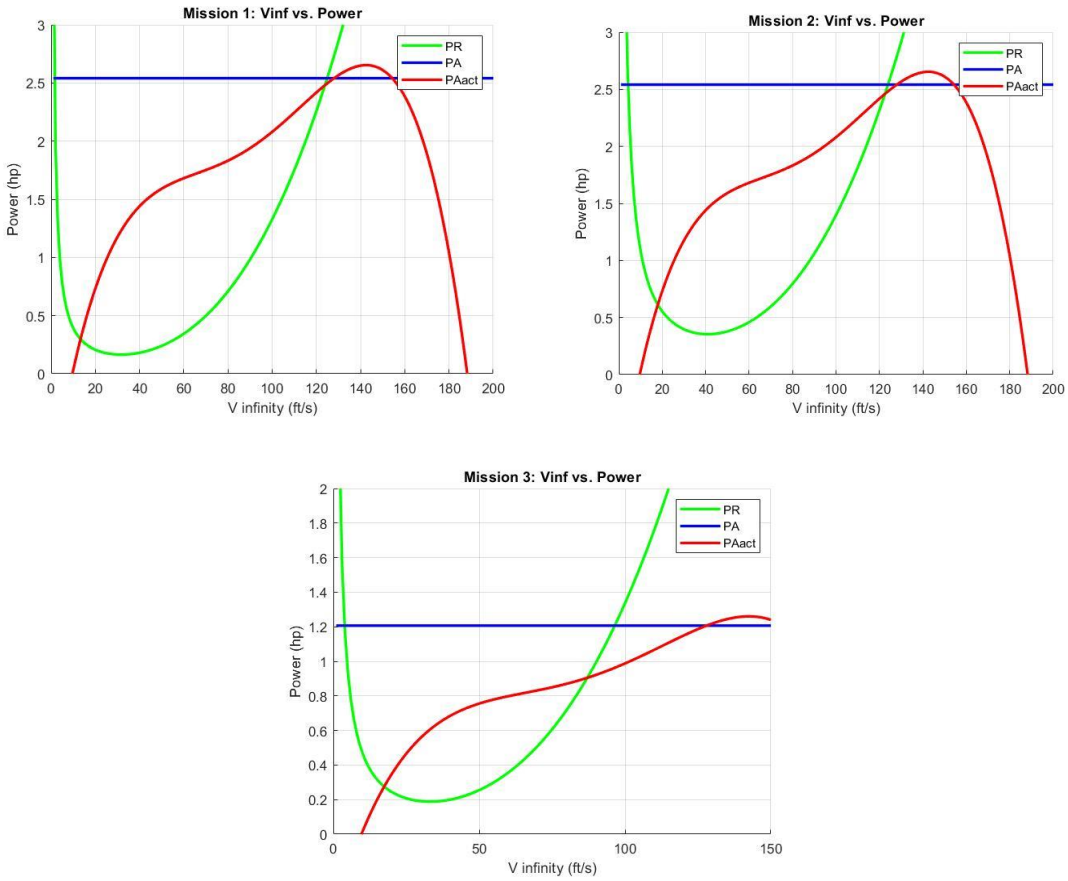

Figure 4.8: Available Power (PA) and Required Power (PR) with respect to Cruise Velocity

From the data above, estimated raw scoring (i.e., pre-normalization) for each of the three missions for the design was calculated. Table 4.4 shows these results, assuming that the airplane cruises at its maximum mission speed for the duration of each mission.

Table 4.4: Estimated Mission Score for Preliminary Design (Not normalized)		
Mission 1	**Mission 2**	**Mission 3**
1	**1.09**	**47.5**

V. Detail Design

A. Dimensional parameters

The final dimensional parameters are summarized in Table 5.1. The fuselage was designed to accommodate the electronics and the shipping containers while maintaining a well-balanced center of gravity. The wing dimensions were based on maximizing wingspan, maintaining a reasonable wing loading, and ensuring a sufficient thickness through the entirety of the wing structure. The tail was sized using historical data on tail volume as well as input from an experienced RC pilot.

Table 5.1: Dimensions of Final Design

Overall Dimensions		**Wing Dimensions**	
Length	5.93 ft	Chord Length	21.16 in. root 12.5 in. tip
CG Location (M1, M2, M3)	18.77, 21.77, 19.69 in.	Wingspan	60 in.
Neutral Point Location	25.13 in.	Wing Area	7.01 ft^2
C/4 of Wing Location	18.51 in.	Aspect Ratio	3.57
Horizontal Stabilizer		**Vertical Stabilizer**	
Chord Length	12.81 in. root 5 in. tip	Chord Length	10.375 in.
Stabilizer Span	26.77 in.	Stabilizer Span	10.375 in
C/4 of Stabilizer Location	51.88 in.		

B. Structural Characteristics

Initial estimates of the airframe structural capabilities were made largely by previous experience. Prototype 1 was constructed with panels of laser-cut balsa wood, each designed according to prior experience and best guesses. After the crash of this prototype, the wreckage was observed (Fig. 5.1), and it was noted that most of the damage occurred along glue lines, rather than along the panels themselves. This suggested that the structure was strong and well-designed, so the same approach is used for the panels of the fuselage of the competition airplane.

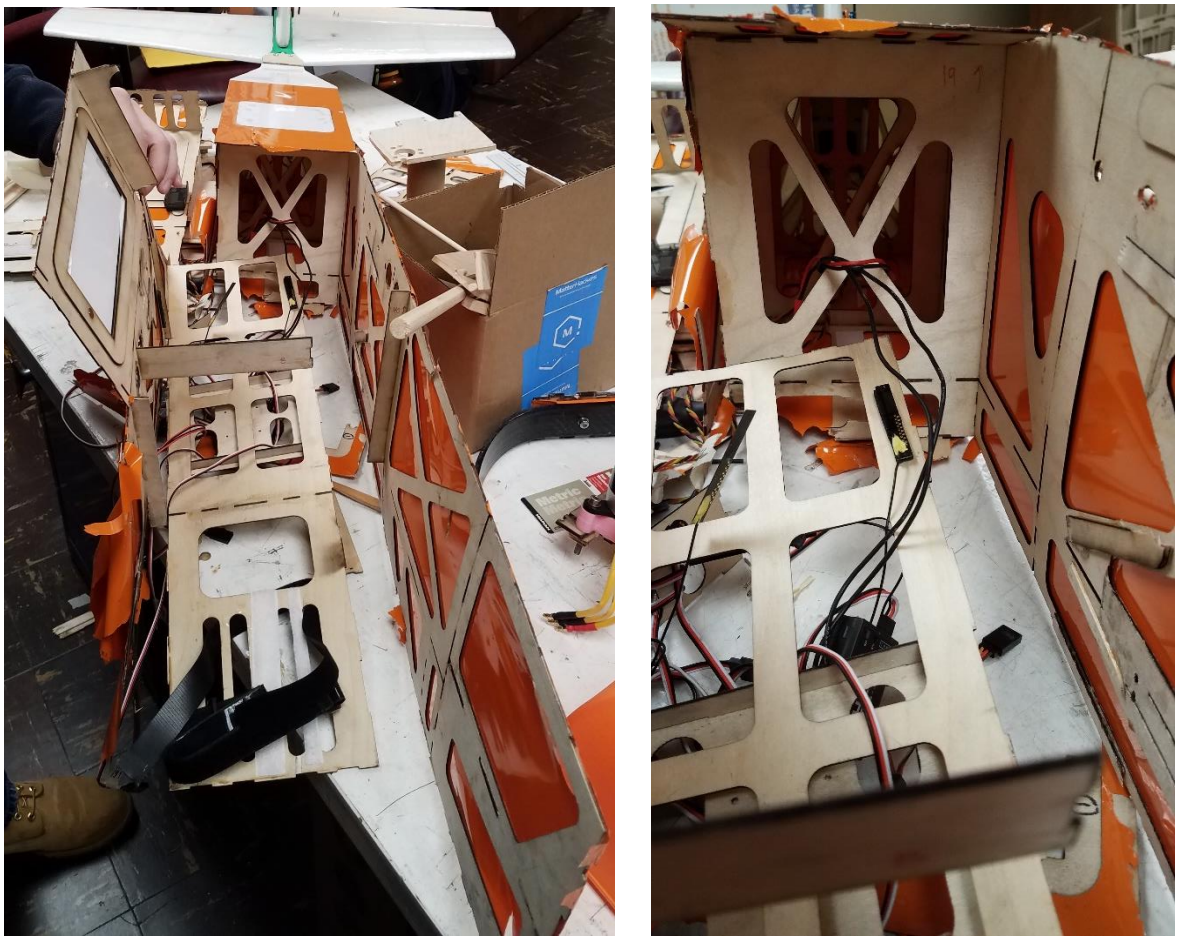

Figure 5.1: Images of the wreckage of Prototype 1, showing close-ups of the points of failure.

C. Systems and Sub-systems Selection and Integration

- Sensor Structure and Stability- Of the various prototype sensors discussed in the preliminary design section, the sensor with the half prolate spheroid nose and external tail fins was chosen as the final sensor. As all of the prototypes were similar in weight, length, and diameter, the decision was made purely based on aerodynamic stability while in tow. As discussed in the testing plan subsection, the sensor with the external fins was the most aerodynamically stable design, in that, while in flight, it stayed nose into the wind, and had little to no flutter in its motion. The sensor has a body with an external diameter (without fins) of 1.5 inches(2.5 inches with fins), a body length of 6.5 inches, and an overall length of 10 inches. It has a weight of roughly 8 ounces, which was our goal weight. The body has 3 openings cut into one side to allow for the placement of LEDs within the sensor, and the nose cone is easily removeable to allow access to the internal circuitry. Both the nose cone and tail cone are made of 3D printed PLA, where the body is made of a length of cardboard tubing.
- Sensor Circuit- The primary goal of the circuit design was to be as compact as possible. To this end, the wires were cut as short as possible. However, because the transistor legs were brittle and broke easily when bent beyond 45 degrees, additional wiring was needed (i.e., so that the legs would not have to bend more than 45 degrees). Since the wires were soldered and closely packed together, short circuits caused erratic behavior, such as turning the LED lights on at random moments or not responding to the transmitter signal. This problem was mainly resolved after careful attachment of

electrical tape on exposed copper wires. Holders for securing the circuitry inside the cardboard tube were considered, but this was not included in the final design due to spacing constraints.

- Deployment Mechanism- The deployment mechanism was designed to accommodate the sensor in both its Mission 2 (i.e., inside its shipping container) and Mission 3 (i.e., ready to be deployed) configurations. The prototype deployment mechanism was a box made of quarter-inch plywood measuring 4.2” x 4.75” x 12.5” on the outside, allowing room for both the prototype sensor (1.67” outer diameter, 7” long main body, with four, 2.5” diameter external fins) as well as the final sensor (1.5” outer diameter, 6” long main body, with four, similar fins). The winch consisted of a dowel supported from the ceiling of the box by two bearings and powered by a continuous servo (right side of Fig. 5.2). The signal wire, which ran from the airplane’s radio receiver to the Arduino microcontroller inside the sensor, required a rotating electrical connection in order to maintain contact between the sensor side of the winch (the rotary side) and the receiver side of the winch (the fixed side). A slip ring was used for this purpose, attaching to the winch at its axis of rotation through a drilled channel in the wood. The winch’s rotation controlled the length of the electrical cabling as well as the length of the tow cable (the yellow braided line in Fig. 5.2). Two servos powered doors on the bottom of the deployment system, as shown in Figure 5.2 below.

Figure 5.2: Prototype Deployment Mechanism (Bottom View).

The original intent was for this deployment mechanism to be mounted inside the fuselage of the competition airplane, but given the destruction of the deployment mechanism during the second flight test, it was decided to take the opportunity to rebuild the mechanism with lessons learned from the construction of the prototype. However, these difficulties were manufacturing-related rather than design-related, so no significant changes were made to the CAD design. Fig 5.3 shows the CAD design for the final deployment mechanism, including a cutaway view to illustrate the winch and bearings.

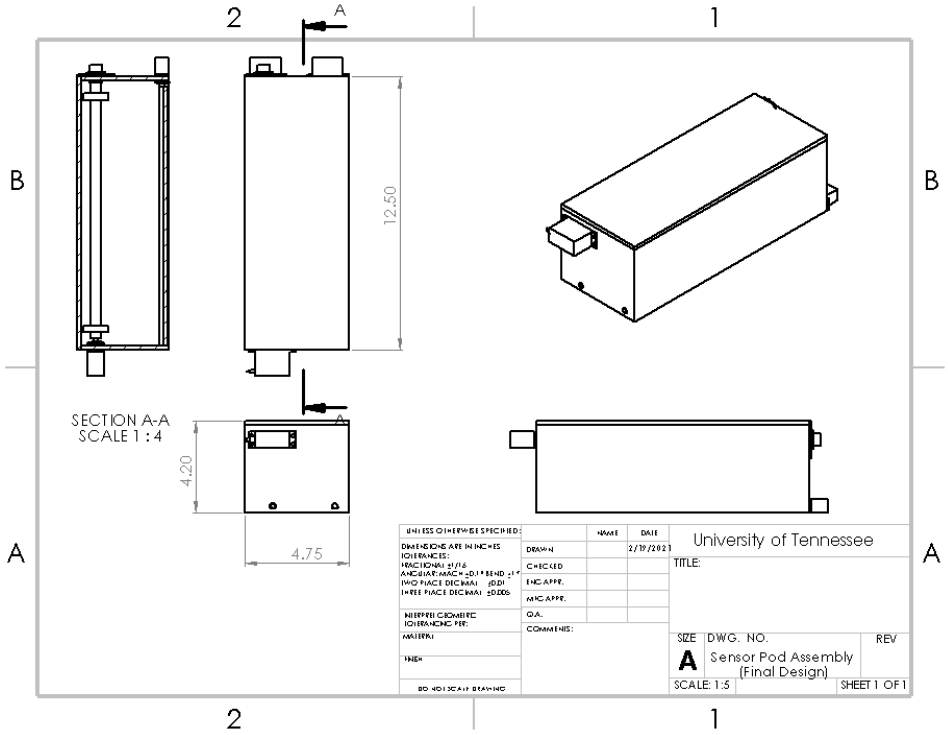

Figure 5.3: Final deployment mechanism to be integrated into the fuselage of the competition plane.

- Integration of Sensor Subsystems- A high score for Missions 2 and 3 required a successful integration of the four sensor components (the deployment mechanism, the sensor body, the sensor circuitry, and the shipping container). The two configurations for the sensor system (Mission 2 and Mission 3) were considered separately.

  In the Mission 2 configuration, no electrical connections were necessary. The sensor will be held in its shipping container with packing material, and the shipping container will be held in the deployment mechanism with the door servos closed.

  In the Mission 3 configuration, there were several connections to make, both physical and electrical. First, an electrical connection was made between the sensor circuit and the airplane receiver by using a slip ring in the winch (26 AWG wire will be used to connect the slip ring to the sensor circuit, and a female-to-female wire will be used to connect the other end of the slip ring to the receiver in the airplane). Second, the physical connection between the sensor circuit and sensor body was made with friction. The physical connection between the deployment mechanism and the sensor body was made with a braided tow cable, which was tied and glued to the winch. The physical connection between the deployment mechanism and the fuselage will be made with bolts.

- Avionics/Electronics- The aircraft is configured with a 2S Turnigy 25C LiPo battery that operates independently from the propulsion system to power the servos and receiver. The battery applied 7.4V to all five high voltage metal gear mini servos allowing for 190.3 oz-in of torque to operate the ailerons, elevators, and rudder. Using the BlueBird BMS-A920 HV servos allows for reliable maneuverability at high speeds and quick response times. The servos are controlled by using two FrSky X8R 8-channel receivers. This allows for a total 16 channels which will operate the servos, ESC, deployment

and recovery mechanism, and the Arduino input signal. The FrSky Taranis X9d Plus is a 24-channel transmitter optimal for the complexity of the flight objectives. This is summarized in Table 5.2.

Table 5.2: Avionics/Electronics Components List

Component	Description
Servo Battery	2S Turnigy 25C LiPo 2200mAh
Receiver	(2) FrSky X8R w/ SBUS
Transmitter	Taranis X9d Plus w/ OpenTX
Aileron Servos	(2) BlueBird A920 HV
Rudder Servo	BlueBird A920 HV
Elevator Servos	(2) BlueBird A920 HV

- Propulsion System- The aircraft's propulsion system is powered by two 8S Thunder Power RC ELITE Series 55C LiPo batteries that are connected in a parallel circuit using XT90 connections. The battery system ideally produces a continuous voltage of 29.6V, which can be subject to change under load. The output XT90 connection from the battery is directly connected to the Phoenix Edge HV 120 ESC, which can handle up to 120A of current from the battery. However, the max current drawn from the battery will not attain 120A, ensuring that the ESC is reliable and will not overheat. The ESC is then connected to the receiver and the motor. The MOTROLFLY DM-5320 330KV brushless motor is rated for up to 2700W, and when used in conjunction with the 8S LiPo batteries, it can produce a maximum angular speed of 9768 RPM and handle up to 91.22A. The motor is rated to use propeller diameters of 18" or 19"; based on an analysis of propeller efficiency, the XOAR PJM-E 19x10 Propeller was selected. This is a 19" diameter wooden propeller with a pitch of 10" and is made specifically for electric RC planes. This is summarized in Table 5.3.

Table 5.3: Propulsion System Components List

Component	Description
Motor	MOTROLFLY DM-5320 330KV
Battery	(2) 8S Thunder Power RC ELITE Series 55C LiPo 3300mA-h
ESC	Phoenix Edge HV 120A
Propeller	XOAR PJM-E 19x10 Electric RC Airplane Propeller

D. Weight and Balance

Table 5.4 shows the breakdown of the weight (in pounds) and location (relative to the firewall) of each of the major components of the design. The center of gravity for all three mission configurations is ahead of the neutral point location (25.13 inches) for the airplane, meaning that the design should be aerodynamically stable in flight. The CG location is furthest back in Mission 2, where the simulated sensors contribute significantly to the location of the CG. The "airplane" component consists of the fuselage, wing, landing gear, and stabilizer weight, or the "empty" configuration of the aircraft, and the combined location of these subcomponents' center of gravity.

Table 5.4: CG Breakdown for Each Design Mission Configuration								
Mission 1			**Mission 2**			**Mission 3**		
Component	**Location**	**Weight**	**Component**	**Location**	**Weight**	**Location**	**Location**	**Weight**
Motor	-5.39 in.	1.34	Motor	-5.39 in.	1.34	Motor	-5.39 in.	1.34
Batteries (x2)	4.08 in.	4.08	Batteries (x2)	4.08 in.	4.08	Batteries (x2)	4.08 in.	4.08
Deployment System	40 in.	2	Sim. Sensors	20.6 in.	5.05	Deployment System	40 in.	2
Airplane	23.2 in.	7.68	Deployment System	40 in.	2	Airplane	23.2 in.	7.68
			Airplane	23.2 in.	7.68			
CG Location	**18.78 in.**		**CG Location**	**21.77 in.**		**CG Location**	**19.69 in.**	

E. Flight Performance

The design's maximum velocity, climb performance, and stall characteristics were all found using MATLAB simulation, and these results were validated using prototype flight testing. Table 5.5 summarizes the predicted maximum velocity for Missions 1, 2, and 3 in their respective flight configurations. The calculation assumes that the propulsion system can maintain this velocity for the entire duration of the mission.

Table 5.5: Maximum Cruise Velocity for Final Design		
Mission 1	**Mission 2**	**Mission 3**
123 ft/s	**122 ft/s**	**87 ft/s**

Table 5.6 shows the stall characteristics of the final design in each mission configuration. This factor largely determines takeoff distance, because the plane must reach stall speed before liftoff, as well as landing speed, because the plane must be above stall speed while airborne. As expected, stall speed increases as the weight of the payload increases, with Mission 1 having the lowest stall speed followed closely by Mission 3 and then a significant increase for the stall speed of Mission 2, where the plane must also carry all the simulated sensors. The stall speed for Mission 3 assumes an undeployed sensor, since stall speed is mainly a concern during takeoff and landing, when the sensor will be fully retracted.

Table 5.6: Stall Velocity for Final Design		
Mission 1	**Mission 2**	**Mission 3**
37.45 ft/s	**46.89 ft/s**	**37.99 ft/s**

Finally, Figure 5.4 shows the climb performance of the design in each of the three mission configurations. As shown, the aircraft performs the best in the first mission configuration where, the actual rate of climb peaks at approximately 60 ft/s and the rate of climb assuming a constant propellor efficiency peaks at over 100 ft/s. For mission two, the actual rate of climb peaks at approximately 35 ft/s and the rate of climb assuming a constant propellor efficiency peaks at 60 ft/s. This is due to the added weight of the sensor and simulated sensors, which requires more power to maintain steady, level flight and thus has less excess power available for climb. Finally, for mission 3 with a deployed sensor, the maximum actual rate of climb was calculated to be approximately 22 ft/s and the maximum rate of climb assuming a constant propellor efficiency is approximately 43 ft/s. Despite being lighter than the mission two configuration, the added drag from the deployed sensor significantly decreases climb performance, as much more power is required to maintain steady, level flight.

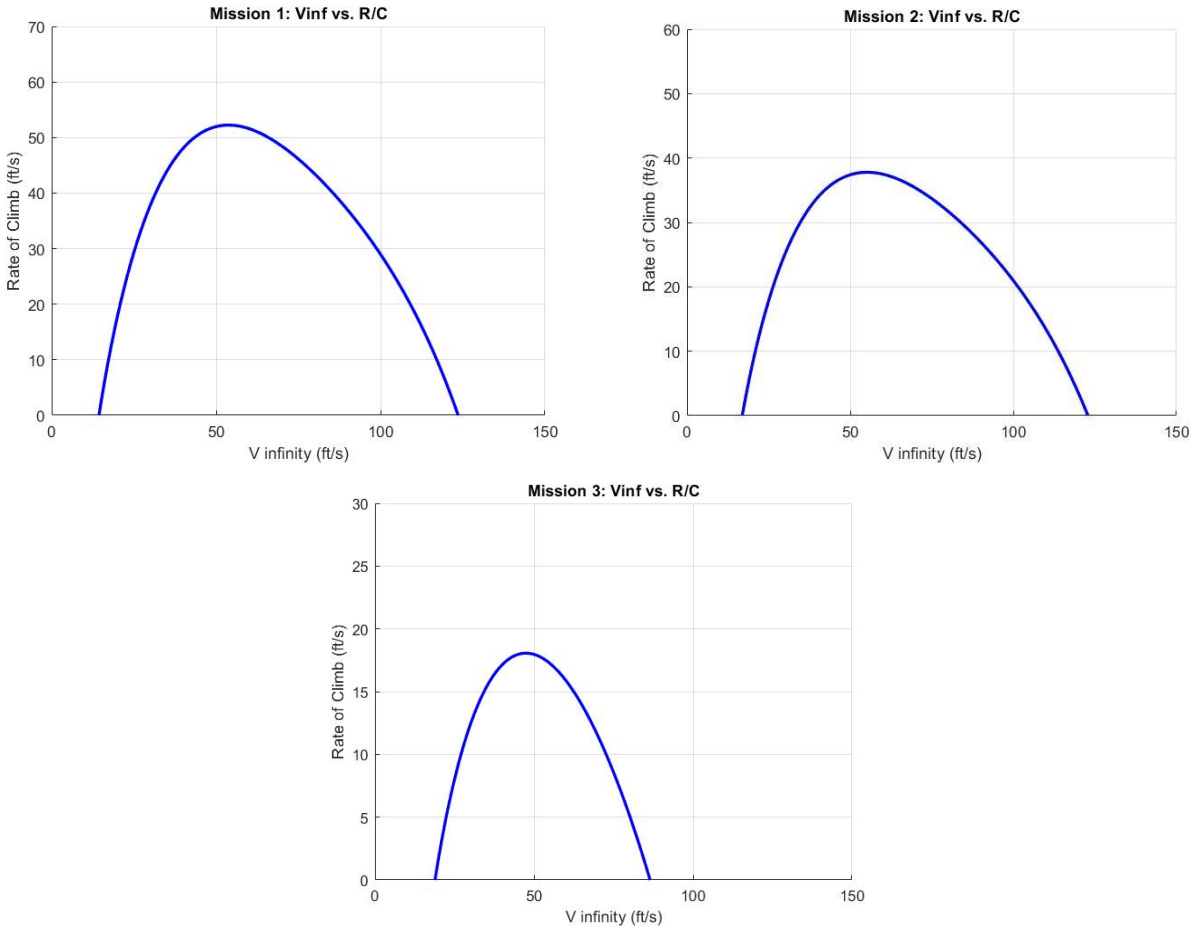

Figure 5.4: Rate of Climb with respect to Velocity for Mission 1, 2, and 3 (Left, Right, and Bottom)

F. Mission Performance

Table 5.7 below summarizes the takeoff performance for the aircraft in each of the mission configurations, using Eq. 5, a rule of thumb for estimating takeoff speed [9].

$$v_{takeoff} = 1.1 * v_{stall} \tag{5}$$

This shows that even in its heaviest configuration, the design still meets the 100-foot takeoff length requirement. The takeoff time and speed are used as part of the acceleration curve in order to more accurately predict our mission score.

Table 5.7: Takeoff Performance

Takeoff	Velocity (ft/s)	Thrust (lbf)	Distance (ft)	Time (sec)
Mission 1	39.96	21.67	26.35	2.71
Mission 2	51.58	20.64	61.83	3.76
Mission 3	41.79	10.27	51.24	3.81

Using fitted functions for the inflight acceleration, the time and horizontal distance traveled can be determined up to reaching the estimated cruise velocity for each mission. By assuming a constant cruise speed, the remaining time and distance is found, and then added to the takeoff and acceleration time and distance to get the overall time and/or distance needed to determine the score for each of the three missions. In mission 3 it is ideally decided that the sensor is to be deployed at 100ft in relative altitude. This allows for acceleration to be greater after the initial takeoff as well as ensuring the sensor will

not affected by the climb. In Table 5.8, the “Before Deploy” column displays the velocity attained by the time 100ft is reached, along with the time and horizontal distance traveled in this period. Once the sensor is deployed the “After Deploy” column of the table shows the cruise velocity that will ideally be maintained throughout the duration of the mission, as well as the time and distance need to accelerate to this speed. Using the remaining allowable time, total distance can be determined for Mission 3 and then converted to the number of laps completed to find the ideal score for the mission.

Table 5.8: Inflight Performance

Mission 1		**Mission 2**	
Cruise Velocity	123 ft/s	**Cruise Velocity**	122 ft/s
Accel. Time	6.3 sec	**Accel. Time**	9.81 sec
Accel. Distance	617.78 ft	**Accel. Distance**	966.56 ft
Remaining Dist.	11355.87 ft	**Remaining Dist.**	10971.61 ft
Total Time	99.3 sec	**Total Time**	101.5 sec
Total Score	1	**Total Score**	1.09
Mission 3	**Before Deploy**	**After Deploy**	
Velocity	73.69 ft/s	87 ft/s	
Accel. Time	4.03 sec	10.774 sec	
Accel. Distance	245.92 ft	900.969 ft	
Remaining Time	-	583.385 sec	
Total Distance	-	51952.667 ft	
Total Score	47.5		

G. CAD Drawing

After the proposal, the CAD model for the final design of the 2020 DBF plane was modified. The plane used for the 2020 competition was a bi-wing plane with large fuselage. To complete this year's missions, the team decided to go with single wing plane with long and little skinny fuselage. The team also decided to use the wings, horizontal stabilizer, and vertical stabilizer for the first prototype. It was learned by this year's team that the wing mount can be easily modified while the tail attachment to the fuselage needed to be redesigned. Thus, for the first prototype, the CAD team, redesigned the model on Onshape with the same wing and tail profile.

- Prototype- For the first prototype, tail section of the plane had to be redesigned so that the tail from last year can be used for this prototype. The CAD and the wing frame team decided to design and create a 2-piece 3D printed part that would attach the tail to the fuselage of the prototype. The 3D printed part would attach the horizontal and vertical stabilizer, and then the pat will be screwed to the fuselage using nylon nuts and bolts.

  To make the design easier, the CAD team decided to only make the plane wing frame symmetric. This way only half the fuselage needs to be design and the other half can be mirrored. Once the plane is mirrored, internal components such as the battery, flight controller, motor, etc. were added to the drawing. It was found by last year’s team that the center of gravity was very close to the neutral point of the plane, so to add more stability to the plane, the team decided to add a motor mount in front of the firewall to move the center of gravity towards the nose of the plane while also keeping in mind that the plane is not too nose heavy.

  The shape and the length of the fuselage were kept the same to avoid complexity for the prototype, however the width of the fuselage was decreased to eliminate extra space. The fuselage shape that previous team designed had many tapered sections to reduce the drag of the airplane. The fuselage was designed to portray the two different thickness balsa wood used for construction. Majority of the fuselage along with internal supports were designed to use 1/16” thick balsa wood and some were designed to use 1/8” thick balsa wood. Additionally, some parts such as the cowling and the motor attachment were designed to be 3D printed. The walls and internal supports of the fuselage were hollowed out to reduce

the weight of the plane as seen in Figure X below. Moreover, the top and the bottom of the fuselage contained many entry panels for the ease of access to the inside of the fuselage. Lastly, on all parts that were merged together, “Laser Joint” feature was used on the Onshape model, so that the assembly is easier to construct.

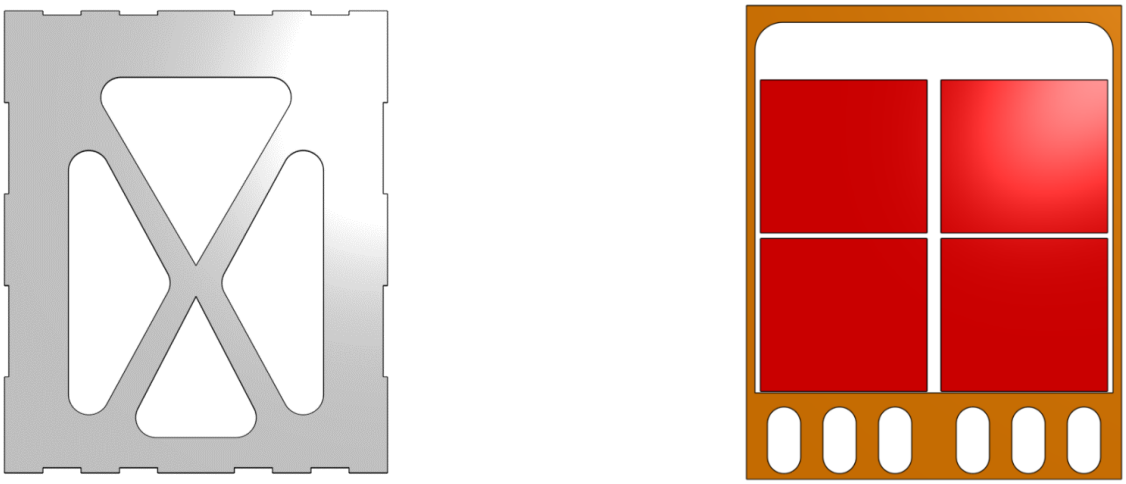

Figure 5.5: CAD modeling element for fuselage of the Prototype (left) and final design (right)

For identifying, the wing and tail location in the CAD design, the airfoil profile were generated form the data points collected form the NACA website [10]. With the profile generated, it was easier to figure out where the carbon fiber rods holes would be placed on the fuselage. To test the wing at different locations, two different rod holes were designed that were about an inch apart. Similarly, the horizontal and vertical stabilizer airfoil profiles were generated to find the location the tail where the tail will attach to the 3D printed part.

Final Design- The final design for the fuselage was decided after the sensor team figured out the container dimension for the sensors. The sensor team decided to have the container dimensions to be 3”x3”x12”, so the width of the fuselage was decided to be 6.625”. This accounts for the Velcro straps to fastens the container, and the wall thickness of the fuselage. Now, the prototype design was modified to fit at least 10 to 12 shipping containers. First, a horizontal support/platform was created in the fuselage where the sensors and the battery will be placed. Since this is where majority of the weight will be, the platform will have a thickness of 1/8’’. Next, for the vertical supports, a rectangular cross section was extruded instead of triangular section, so the sensors can be stacked on top of each other as seen in Figure 5.5. Then, similar to the prototype new wing and tail airfoil profiles were generated to find the location of where the carbon fiber rods will fit. For the tail, the team decided to go with a fixed tail which is integrated into the fuselage instead of on a detachable tail mounted on the 3D printed part. Having a fixed tail to the fuselage will not strengthen the tail structure, but it will also decrease the weight of the airplane. Next, the sensor deployment system as seen in Figure 5.2 was incorporated into the design. The deployment system is placed toward the rear of the fuselage, and on the bottom, it will have “bomb bay” door that open out to deploy the sensor for mission 3. Next, new cowling for the motor was designed with a cut-out piece at the bottom to prevent the motor from overheating. Lastly, again similar to the prototype, “Laser Joint” feature was used for the ease of constructing the assembly.

Drawing Package

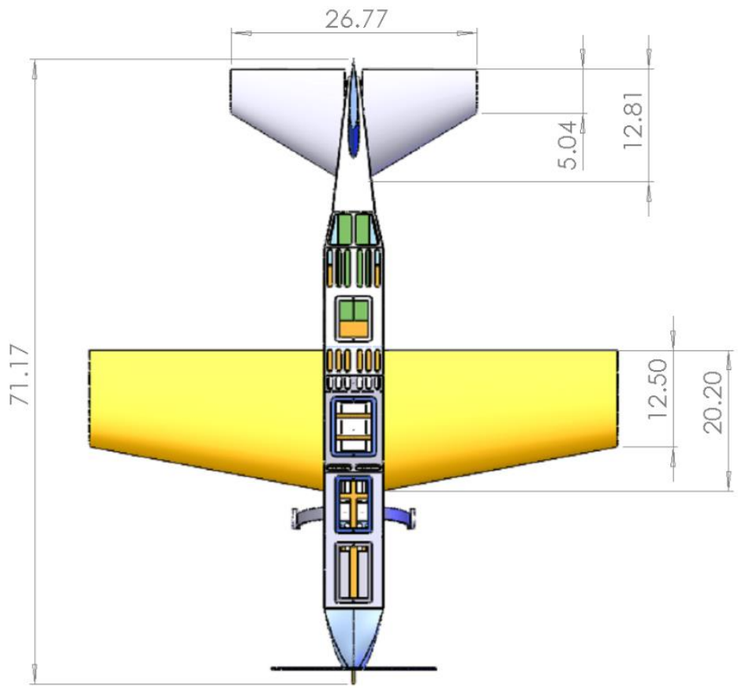

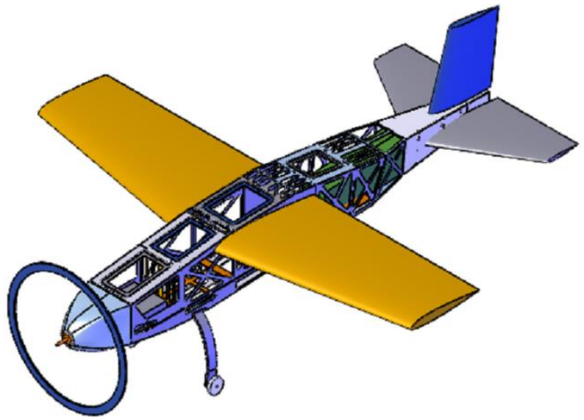

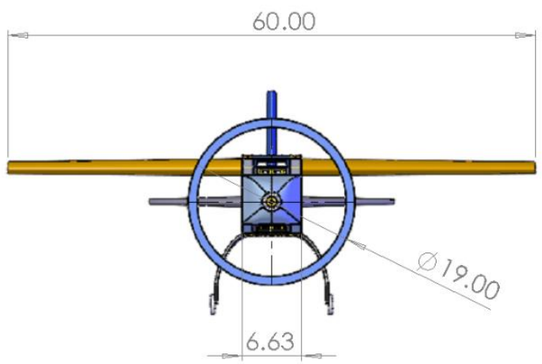

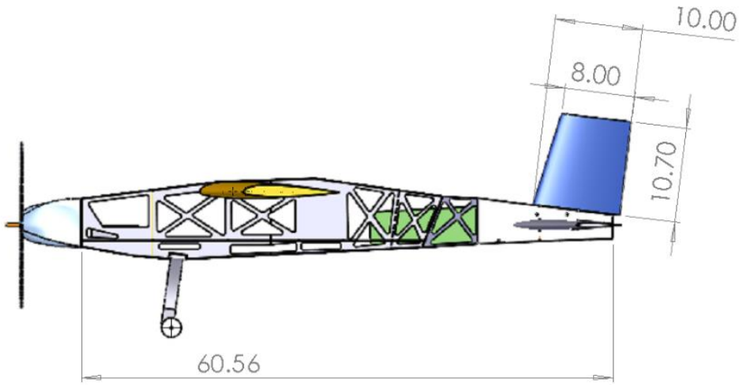

TITLE: Orthographic and Isometric View for M1 and M3			
SIZE B	DWG. NO. Final Design		REV
SCALE: 1:16	WEIGHT:	SHEET 1 OF 1	

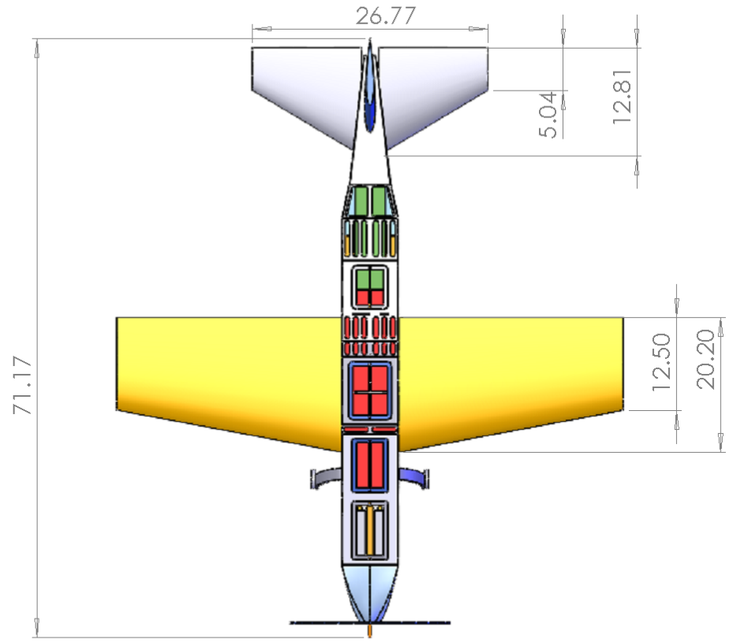

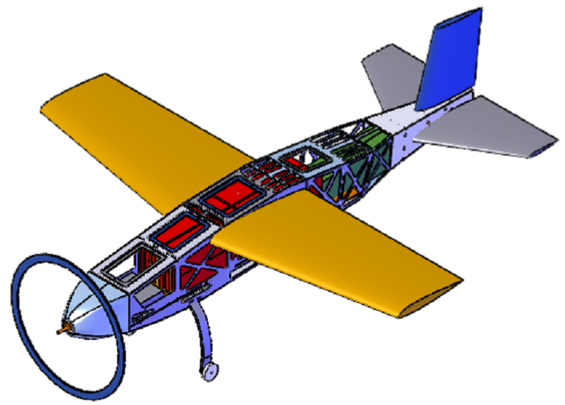

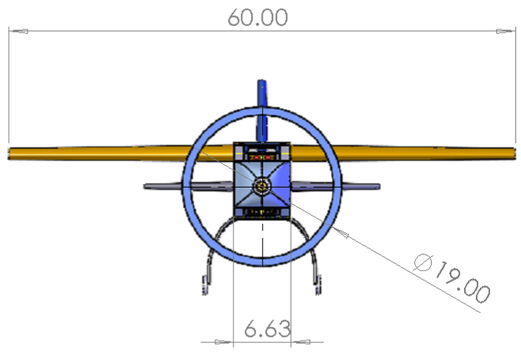

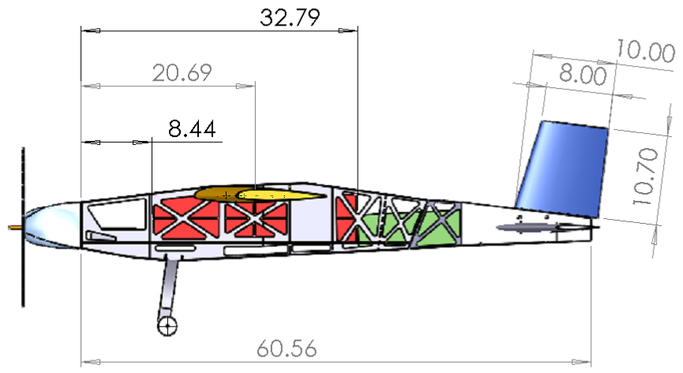

TITLE:
Orthographic and Isographic View for M2

SIZE	DWG. NO.	REV
B	Final Design	

SCALE: 1:16 WEIGHT: SHEET 1 OF 1

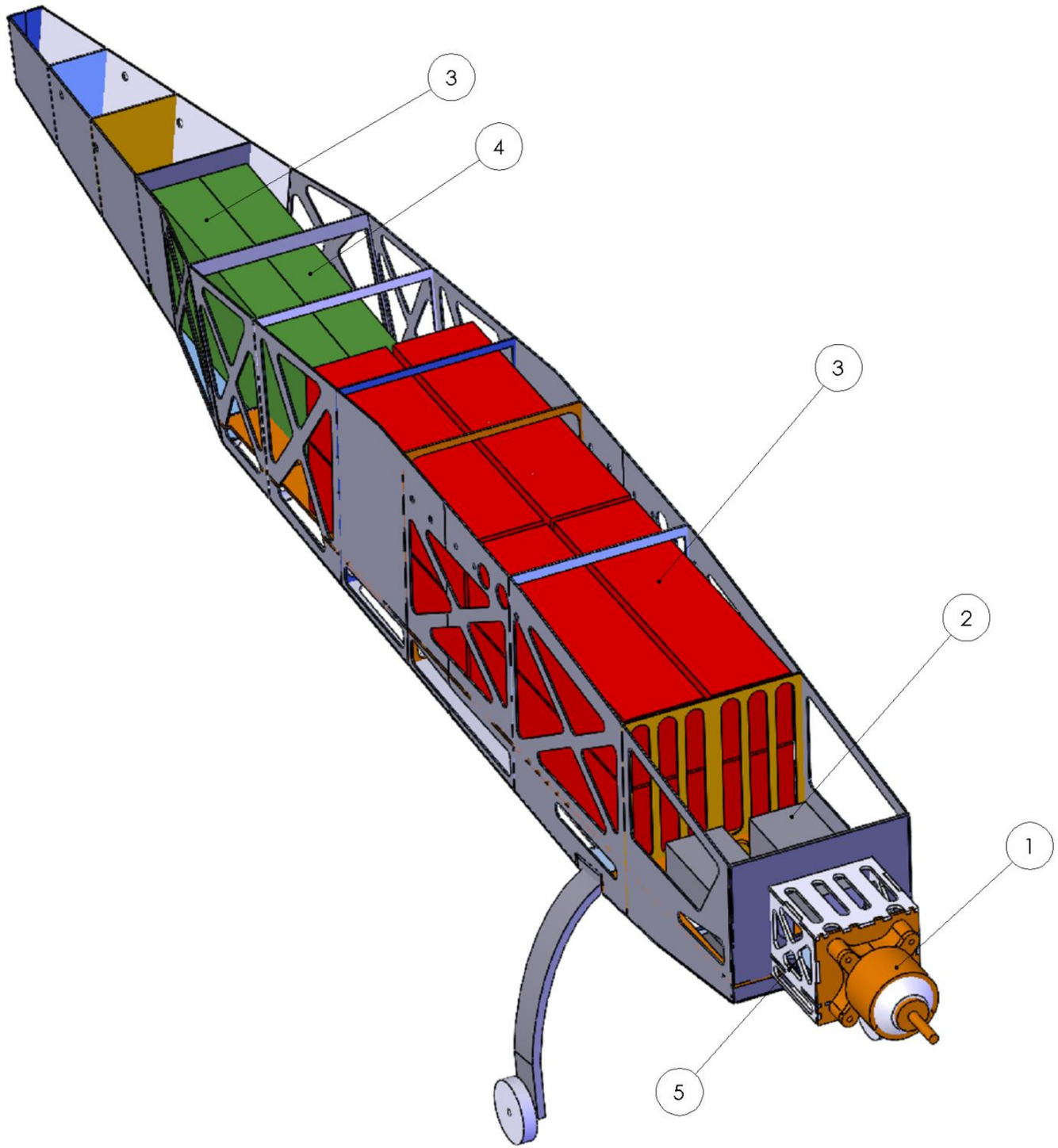

Number	Name	Quantity
1	Motor	1
2	Battery	2
3	Sensors	9
4	Deployment System	1
5	ESC	1

*Note: One sensor is inside the Deployment System

TITLE:
Inner Fuselage

SIZE	DWG. NO.	REV
B	Final Design	

SCALE: 1:8 | WEIGHT: | SHEET 1 OF 1

VI. Manufacturing Plan

Several different manufacturing processes for each component of the aircraft were investigated in the course of our design process. Using historical data from previous Design, Build, Fly teams as well as advice from team members with RC experience, each of these processes were analyzed and eventually a manufacturing plan for each major component of the aircraft and payload was selected.

Possible Manufacturing Processes

- Balsa Build Up – Balsa construction is a common manufacturing method for RC aircraft as it can be relatively easy to do, creates a relatively strong frame, and is one of the lightest methods for building aircraft structures because of the low density of balsa. However, without experience in using balsa, it can be difficult to get high fidelity components using this method and is not as strong as some of the other methods considered.
- 3D Printing – 3D printing results in high fidelity parts since the manufacturing is done through a CAD model by a computer. While the resulting parts are also very strong, the material is too heavy to be considered for any of the main structural components of the aircraft. However, 3D printing was a great option for printing smaller complex components on both the airplane as well as the sensor.
- Laser Printing Lite Plywood – Laser printing plywood results in a structure like that of balsa construction, but with a higher degree of accuracy because all components can be modeled in CAD with laser cut joints, which then allow the pieces to fit seamlessly together during the construction phase. Lite Ply ® construction results in a slightly heavier component than balsa, but the resulting product is also stronger due to the material properties as well as the tightly connected laser-printed joints.
- Composites – Composite manufacturing results in an extremely durable part with a relatively low weight, although it weighs more than both the balsa and plywood manufacturing. The manufacturing process is also more complex and time consuming, and it can sometimes be difficult to get high fidelity parts without experience with composites. Due to the time constraints as well as high cost of this manufacturing method, it would not be ideal for major components of the airplane. However, it was used in parts that needed to be more durable, such as the landing gear.
- Foam – Foam construction is one of the easiest methods to make more complex structures by hand. However, the resulting parts must be reinforced with some sort of sheeting or supports added inside of the foam, making it generally heavier than balsa or plywood components. Team members have also had past experience in making components like the wing and stabilizers out of foam, meaning that a higher fidelity part could be made using this manufacturing process.

Selected Manufacturing Process by Component

- Wing – A polystyrene foam core wing with a balsa skin was selected for the wing of our design. By using a hotwire and template, the foam could be cut to the desired airfoil shape more precisely than other manufacturing methods such as a balsa build up or laser cutting, where MonoKote can easily warp and twist the wing shape. A balsa skin applied over the foam core then allowed for a smooth surface of the wing, reducing the coefficient of skin friction and thus the skin drag of the airplane. A phenolic tube is inserted into the wing so that the carbon fiber wing spar can slide into the foam core. The leading and trailing edge of the wing are constructed using balsa epoxied onto the front and back of the foam core that is sanded to the correct shape. Ailerons, elevators, and the rudder are constructed of balsa and attached using nylon hinges. A root cap is installed on each wing with wooden pins and a blind nut countersunk into the wing so that the wing can be easily aligned and attached to the fuselage. Smooth balsa tip caps are applied to the wings for increased structural stability

and improved surface characteristics. Finally, the surface of the wing is covered in MonoKote to ensure a smooth finish to the surface of the components.

- Stabilizers – A foam buildup manufacturing method was also chosen for the vertical and horizontal stabilizers, but Expanded Polypropylene (EPP) was chosen as the material rather than polystyrene. EPP was not an option for wing construction because it is not as readily available as polystyrene, but it was feasible to make the stabilizers because of their smaller size. This material is much more durable than polystyrene and allows for a much simpler building process as it is not necessary to skin the foam in balsa after hotwire cutting. After hotwire cutting, carbon fiber spars are inserted into the foam from the roots of the stabilizers, control surfaces and servos are installed on the surfaces of the stabilizers, and they are then skinned in a layer of MonoKote.
- Fuselage – For the fuselage of our final design, a laser printed Lite Plywood construction method was chosen because of the high strength to weight ratio of the material and the high fidelity that laser printing allowed for the components. First, the CAD model shown in the detailed design was broken down by parts, and then a CAMFive laser cutter was used to cut the parts out of 1/8-inch and 1/16-inch Lite Ply ® aircraft spruce. These parts were then sanded and dry fit together. The fuselage was then glued together using Gorilla Wood Glue, clamped, and weighed down to prevent shifting while the glue cured for 24 hours. Finally, the assembled fuselage was sanded once again, electronics were installed, and then MonoKote was applied to the completed fuselage.
- Landing Gear – A carbon fiber composite structure was chosen for the landing gear, manufactured using an infusion molding technique. First, a mold for the infusion was modeled in CAD software and then 3D printed. Epoxy was applied to five layers of carbon fiber, which were then placed on the mold alternating in a zero- and forty-five-degree fiber orientation. In a vacuum bag. A vacuum was then pulled on the mold for twenty-four while the part cured, and the finished component was removed from the bag and sanded to the correct final structure. Wheels were attached to the landing gear using metal pins, and the final assembly was attached to the fuselage using bolts, lock nuts, and epoxy to reinforce the joints around the gear.

Sensor System

- Container – The shipping containers were constructed out of square cardboard mailing tubes due to their light weight and durability. These tubes shipped pre-flattened and were folded into the appropriate rectangular shape upon arrival. A seam of cyanoacrylate was run across the length of the joints of the container to help it retain its shape. Packing paper was crumpled and placed in either end of the container to help absorb impact when dropped on its axial faces. The simulated sensor containers were constructed from the same cardboard mailing tubes using the same methods. Cylindrical cardboard tubes were considered for the sensor containers. However, the square tubes were chosen because they stack more easily within the fuselage of the airplane and pose less of a risk of shifting during flight. The weight of the sensor was obtained using a digital scale. This process was repeated five times, and the weights were averaged together to obtain our final weight. Once the sensor weight was determined, individual plastic bags were filled with lead shot to an equal or slightly greater weight than that of the sensor. Again, this process was repeated a total of five times per bag to ensure the accuracy of our results. One bag of lead shot was placed inside each simulated container and secured using adhesive tape. The sensor containers were secured together in the cargo hold of the aircraft using hook-and-loop fasteners. This prevents the containers from shifting in the cargo hold during flight and causing undesirable effects on the handling of the aircraft.
- Sensor – The sensor was manufactured using materials readily available to the team. The main body of the sensor was constructed of a length of 1.5-inch outer diameter cardboard tubing, cut to the appropriate length using a miter saw to

ensure square edges. Holes were cut into the body tube with razor blades to allow the internally mounted LEDs to be seen from the ground while in flight. Holes were also cut into the body to allow the attachment of both a tow cable and a signal cable, both of which run from the sensor to the aircraft itself. The nose cone and tail fins were 3D printed from PLA. The tail fins were printed separately from the rest of the tail structure and glued into place with CA glue, as a solid, one-piece fin structure proved too brittle. The entire tail fin assembly was then attached to the sensor body with CA glue, while the nose cone was simply inserted and held in place by friction. The nose cone was left detachable to allow for ease of access to the internal circuitry of the sensor.

- Sensor Circuitry- The very first prototype was built using the ELEGOO Uno, three BC547 transistors, three 220 Ohm resistors, and no connection to the receiver. This option was chosen for the familiarity of ELEGOO Uno from previous coursework and the simplicity of circuit without any code dealing with PWM. The prototype circuit is pictured below in Figure 6.1.

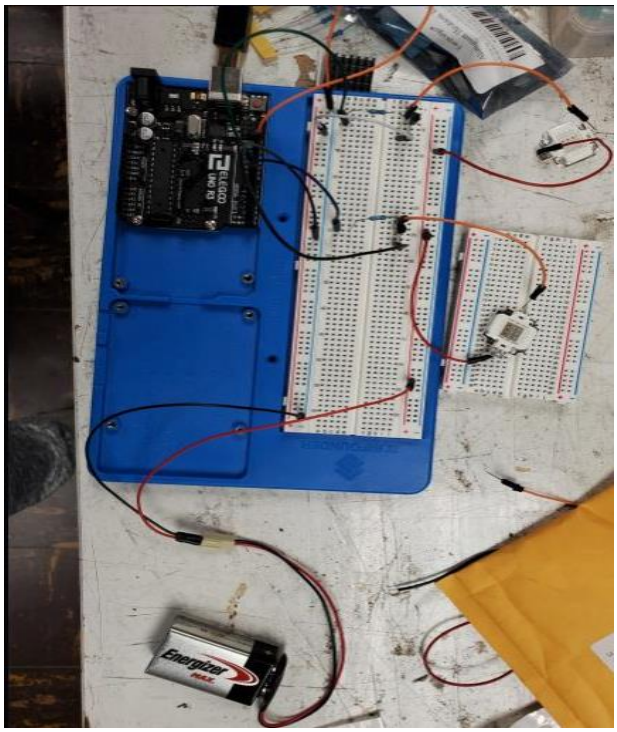

Figure 6.1: First prototype circuit for sensor

To make the circuit as compact as possible, alligator clips for circuit connection were not an option. The only option was to solder the entire circuit. The length of the wire had to be cut to minimize the area filled by the extra useless wires. Furthermore, transistor legs and resistor legs were cut short in order to save space. With adjustable helping hand, solder smoke absorber, and soldering iron and wire, the wires were soldered on the ELEGOO nano, transistor, resistor, and LED. In order to keep the circuit in place and to make it as organized and compact as possible, black electric tape was used. Moreover, black electric tape was covered over exposed copper wires to prevent short circuiting which will malfunction the circuit and to reinforce the circuit to keep it alive for the drop tests. The ELEGOO nano was programmed so that the LED will turn on when the PWM from transmitter is greater than 1700, and the LED will turn off when the PWM from transmitter is smaller than 1300. The final circuit is shown below in Fig. 6.2.

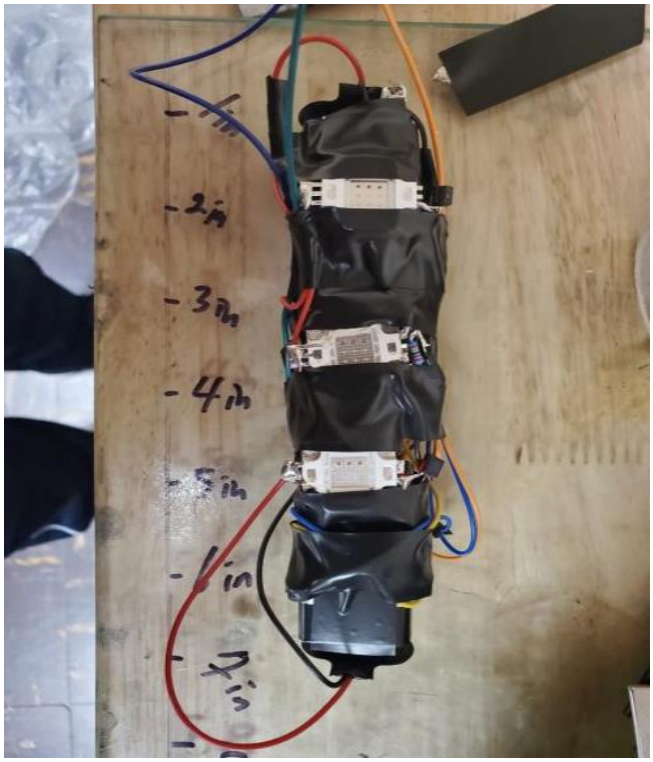

Figure 6.2: Final design for sensor circuitry

- Deployment System- Construction on the deployment mechanism could not begin until dimensions were finalized for the sensor it would contain, so the manufacturing plan was constrained by the sensor aerodynamic testing schedule. The manufacturing plan for the deployment mechanism thus began with a CAD phase, since the general structure and proof-of-concept work could be done while awaiting final dimensions, and then the specific dimensions could be added later.

  To ensure that each part of the deployment mechanism would fit prior to construction, CAD software was first used to study their relative motion. After ensuring that none of the parts would interfere, each was manufactured individually, according to their dimensions in the CAD model. The outer box structure was made of quarter-inch plywood, which was cut to general size on a band saw and then sanded as needed. After each of the panels were cut, internal cuts were made (e.g., to house the continuous servo) by drilling out a large section and then refining the edges with a rotary sander. Five of the six sides of the box were dry-fit (all except the doors on the bottom) and screwed together. Once this outside shape was formed, the internal structure was added. The bearings for the winch were mounted inside plywood supports, which would secure them to the ceiling of the deployment mechanism. The dowel for the winch was cut to length and mounted inside these bearings, which were aligned with the slip ring and continuous servo and screwed into the ceiling. The slip ring and continuous servo were bolted into place. Finally, the door servos were bolted into place, and holes for the door hinges were cut in order to align with the axis of rotation of each servo. Segments of quarter-inch dowel were used as hinges.

  Since this deployment mechanism was destroyed in the second flight test, a second one will be constructed with a similar manufacturing process, except the box will be 3D-printed rather than cut and assembled from plywood. This will alleviate some of the issues encountered with the initial construction process, such as bowing in the dowel used for the winch (this

put added stress on the bearings), since the tolerances required will be easier to achieve with 3D printing than with manual measuring, cutting, sanding, and screwing.

VII. Testing Plan

Extensive testing was performed both on subsystems of the airplane and on the airplane itself in flight. Testing was a critical step in the process of designing and building the plane, allowing the team to evaluate performance and inform future design decisions. Subsystem testing included testing of the propulsion system, the sensor deployment mechanism, and the sensor itself, while flight testing involved evaluating the performance of all systems working concurrently while in flight.

Objectives:

- Propulsion test- Using an Rcbenchmark 1585 thrust stand, the propulsion sub-team performed a series of static propulsion tests on the Motrolfly motor and 8S Thunder Power LiPo battery packs. The team tested motor efficiency vs current, RPMs vs current, and static thrust vs current for two different propellers, a 19x10 and an 18x12. When comparing these two propellers, the greatest considerations were thrust and efficiency. The 19x10 propeller with a larger diameter was expected to have a slightly better efficiency, whereas the 18x12 propeller with the steeper pitcher was expected to create more thrust. The team did not expect RPMs to vary greatly between the two propellers tested. In addition to comparing propellers, the team performed a voltage drop test. These data enabled the team to evaluate performance of the motor and batteries as well as identify the ideal propeller for flight testing.
- Sensor tests – To ensure that the final sensor would perform successfully in the competition, several tests were conducted. These included a stability test, brightness test, deployment test, and container drop test.
    - Sensor stability test – To select the final sensor configuration, each of the various sensors designed by the team were subject to testing in a wing tunnel. However, none of the sensors were stable enough at the initial low speeds to safely continue testing, so a different test was contrived. Each sensor was towed behind a testing rig attached to a pickup truck. This rig consisted of a beam clamped to the bed of the truck, with eyelets in the end of the beam. The sensor was attached to the eyelets with fishing line to simulate how it would be towed from the aircraft. The stability of each sensor was observed, and the most stable sensor was selected for flight testing.
    - Sensor brightness test- To verify that the sensor would satisfy the requirement that the sensor lights be visible during the flight, a brightness test was performed. Because the maximum distance from an observer to the plane at any point during the competition was estimated to be 715 ft, the sensor was taken to the top of a parking garage on a bright day while observers stood 1000 ft away. The test would be considered successful if the light pattern could be seen, and unsuccessful if it could not. An unsuccessful test would lead to a redesign of the current sensor circuitry.
    - Sensor deployment test- To ensure that the deployment mechanism could be successfully operated midflight, the mechanism was tested in the lab. If the deployment mechanism could deploy and retract the sensor without issue, the test would be considered a success. An unsuccessful test would lead to a repair or redesign of the current deployment mechanism.
    - Sensor container drop test- The objective of the drop test was to verify that the shipping container and the sensor could withstand a drop shock event from ten inches and still function properly. In order to verify this, the sensor and container were dropped a total of eighteen times over three tests. First, the sensor was placed within the container, and craft paper was placed at either end of the container to help absorb the impact of the drop. Each face of the sensor container was numbered one through six. A yard stick with inch increments was secured to a blank wall in order to provide an easily visible backdrop for the test. For test one, the sensor plus container were dropped on each

face of the rectangular prism from a height of ten inches. For test two, the sensor plus container were again dropped from a height of ten inches on each face. For test three, the sensor plus container were dropped from a height of fifteen inches on each side. After each test, the sensor was removed from the container, and the circuitry was checked to make sure that the LED lights were still functional. If the sensor could protect the sensor from physical or functional damage, the test would be considered a success. An unsuccessful test would lead to a redesign of the sensor container. A photo of this test is seen in Fig. 7.1.

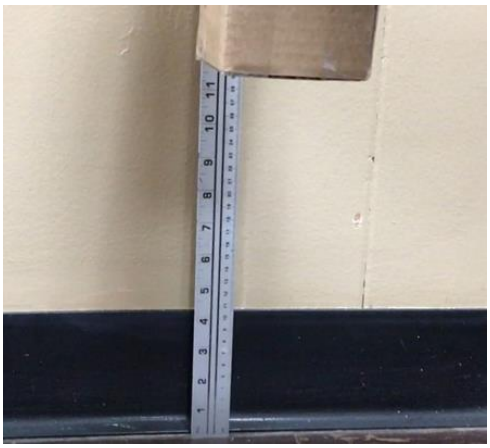

Figure 7.1: Sensor and cargo container during 10 inch drop test

- Flight testing- Once the prototype was built, a series of flight tests were conducted to evaluate the performance of the airplane and its subsystems and to inform future design decisions. In addition, the flight tests were a crucial step to confirm the collaboration of each individual subsystem and prove that the airplane as a whole works.

  The tests were approached with an abundance of safety and caution, so as to protect both the members of the team and the plane itself. Extensive inspections and checklists were followed to uncover all potential issues and avoid accidents at all costs. Each component of the airplane was carefully inspected, and any anomalies would result in the delay of the test flight until the issue was resolved.

  The first test flights of Prototype I followed an iterative process of adding weights to determine ideal wing and power loading. The first flight involved no added weights, then weights were added or removed between flights based on pilot feedback on control authority, stability, and excess power. Despite the prototype not being able to carry as much weight as was desired of the final airplane, determining the ideal wing and power loading provided the team with crucial information on how to design the final airplane to carry enough weight for the competition.

  In addition, the first test flights were also used to measure takeoff distance, stall tendencies, climb performance, and maximum speed at each cargo load. Takeoff distance, stall tendencies, and climb performance were measured by simply observing the plane in flight and recording pilot feedback. Maximum speed was measured by flying full throttle during a portion of the flight, then analyzing airspeed data recorded by the onboard data acquisition system. The data from these tests were used to inform decisions on wing sizing, tail sizing, and cargo capacity.

  The second day of flight testing was designed to first collect more data on takeoff distance, climb performance, and maximum speed while simultaneously collecting voltage and current readings, which were unavailable for the first test flights. The primary goal, however, was to test the sensor deployment mechanism in flight. These results would both confirm that the deployment mechanism works and test the stability of the sensor in flight, which had already been selected

from the stability test described in Section VIII. If the sensor was able to be deployed and towed without issue, these components would continue to be used in the final airplane. If they failed, the components would be redesigned or refined and then tested further.

Flight Test Schedule and Objectives

Table 7.1 below shows a summary of our flight-testing schedule with the date, location, and objectives for each of test.

Table 7.1: Testing Schedule

Date	Location	Objectives
01/30/2021	House Mountain RC, Corryton, TN	Test stability of Prototype. Determine ideal wing and power loading Measure maximum speed and takeoff distance
02/12/2021	Downtown Island Airport, Knoxville, TN	Test stability of various sensors in tow
02/13/2021	University of Tennessee, Knoxville, TN	Confirm pre-flight operation of sensor deployment mechanism
02/14/2021	Knox County RC, Knoxville, TN	Test sensor deployment mechanism
02/17/2021	University of Tennessee, Knoxville, TN	Confirm operation and visibility of sensor lights
02/17/2021	University of Tennessee, Knoxville, TN	Sensor shipping container drop tests

Pre-Flight Checklists

Table 7.2 below shows the pre-flight checklist that was completed before each test, ensuring that the plane ready to fly before a test was conducted and that all data relevant to the test was properly collected and recorded.

Table 7.2: Pre-flight Checklist

Flight Phase	Tasks
Internal Check	❑ Record voltage of flight and receiver batteries ❑ Load and secure batteries and cargo ❑ Ensure wing is secured with wing bolts
Fuselage Check	❑ Check for tears or rips on surface
Landing Gear Check	❑ No visible damage ❑ Landing gear is securely attached ❑ Wheels turn freely
Propulsion System Check	❑ Inspect propeller ❑ Motor is securely mounted
Deployment Mechanism Check (if applicable)	❑ Install deployment mechanism ❑ Check location of CG ❑ Ensure sensor is securely assembled and tied to cable ❑ Ensure tow cable is free from tangles
Control System Check	❑ Check control surface connections ❑ Check pushrod connections ❑ Ensure servos are securely installed and undamaged ❑ Plug in batteries and turn on transmitter ❑ Close hatches ❑ Ensure control surfaces are not binding ❑ Arm airplane ❑ Confirm personnel are behind propeller ❑ Test throttle to maximum

VIII. Performance Results

Following the creation of extensive testing plans, the team began testing the aircraft subsystems and eventually the aircraft itself. Most tests proved very successful either in confirming the operation of subsystems or in gathering useful data, while some tests were less fruitful. However, even these testing failures were valuable in guiding future designs by pinpointing areas of improvement.

Subsystem Testing Results

- Propulsion test results- After completing the various propulsion systems tests, the team compiled and plotted the results. As shown in Figure 8.1, the RPMs of the motor with each propeller installed were very similar, as expected since both propellors were of similar size and weight.

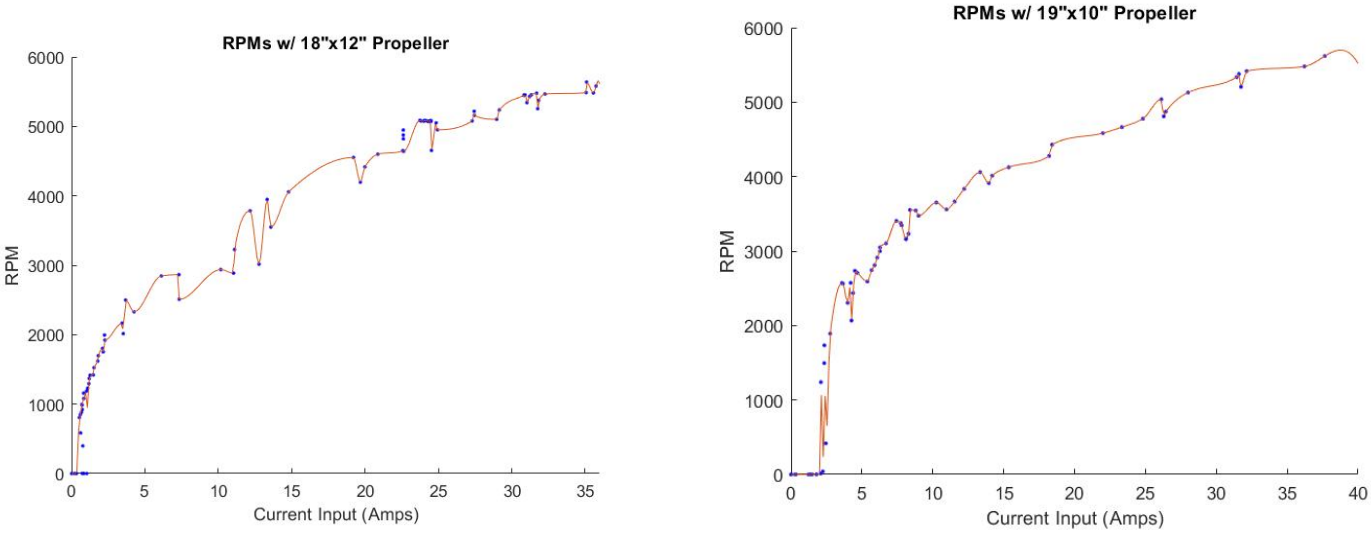

Figure 8.1: RPM with 18x12 Propeller (L) and 19x10 Propeller (R)

When comparing static thrust, shown in Figure 8.2, the 18x12 propeller can be seen to produce slightly greater thrust for a given current input. This was also expected, as the 18x12 propeller boasts a slightly greater pitch and thus will move more air during each rotation of the propellor.

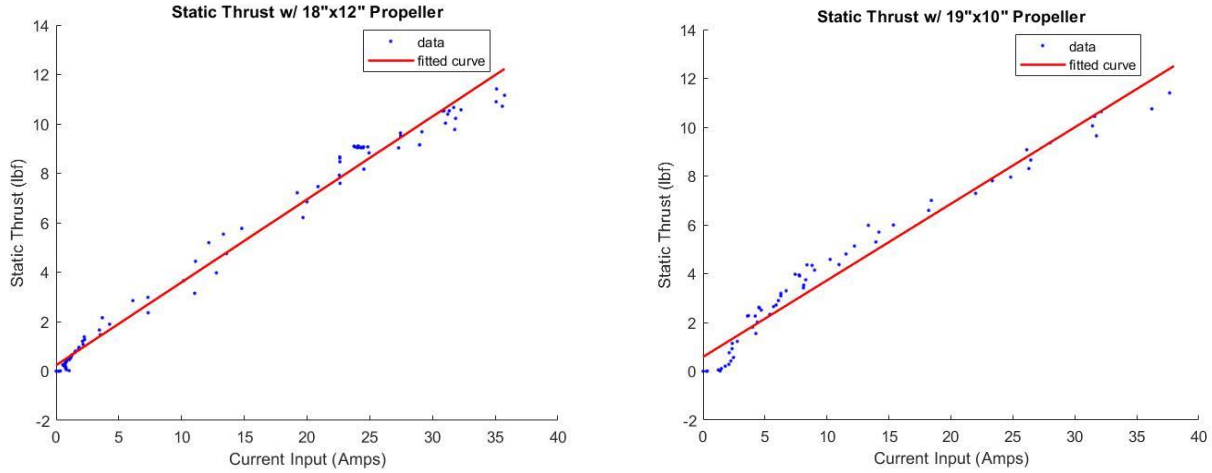

Figure 8.2: Static Thrust with 18x12 Propeller (L) and 19x10 Propeller (R)

Finally, motor efficiency data was collected using an optical RPM probe on the RCBenchmark Test Stand. In order to find this, the mechanical power output was measured in comparison to the electrical power input to determine the mechanical efficiency. As the current coming to the motor increased the data portrayed a logarithmic curve, as shown on Figure 8.3. The voltage drop test, seen in Figure 8.4, displays two different relationships, voltage vs. current and voltage vs. time. The relationship between voltage and current is present in the slope of the points in the figure, since as current is increased the voltage will drop more quickly compared to when current draw is small. The voltage drop over time can be seen directly on the graph, and is approximately a linear relationship when current draw is constant. The current was not increased at a constant rate, so Figure 8.4 cannot be given a curve fit.

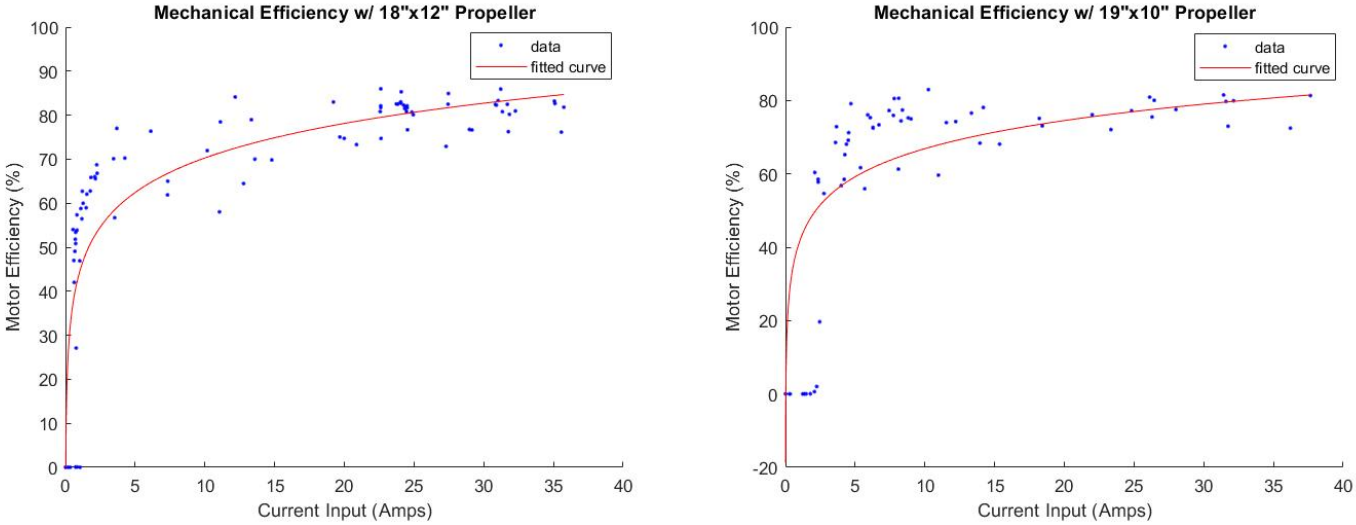

Figure 8.3: Mechanical Efficiency with 18x12 Propeller (top) and 19x10 Propeller (bottom)

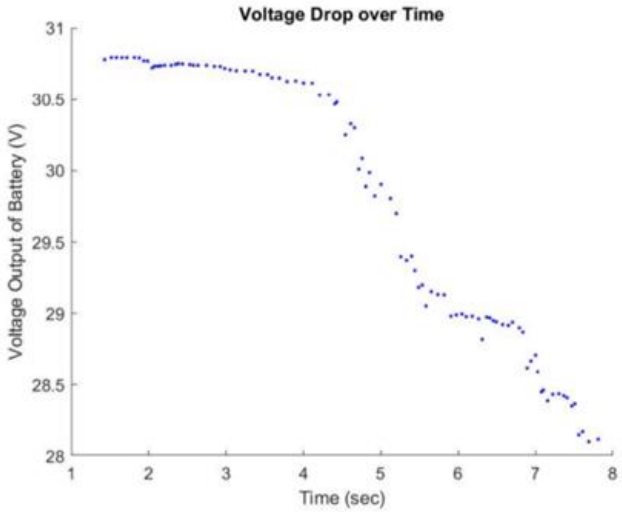

Figure 8.4: Voltage drop over time for thrust stand testing

- Sensor Testing- After the first sensor drop test, carried out from a height of 10 inches, the sensor circuitry did not light the LEDs. This was likely due to a bad ground within the wiring. The circuit was readjusted, and the LEDs were verified to be working correctly. After test two, also from a height of 10 inches, the sensor circuitry functioned properly, and all lights flashed in their designated pattern. After test three, this time from a drop height of 15 inches, the sensor functioned properly for the most part. Two of the three LEDs responded to the incoming signal and flashed appropriately. The third

LED did not light at all. It is suspected that there was once again a bad connection causing the third LED to not work correctly. These tests demonstrated a lack of reliability in the sensor circuit, which will require correction to achieve a desired level of reliability. The circuit containing the LEDs will be made more robust to allow a greater chance of survival after the drop test.

The initial prediction that the LEDs would be visible at 1000 ft during the brightness test proved to be highly inaccurate. On the day that the test was conducted, the lights were only visible at distances of around 100 ft, and even then, only the red light was visible. Two other LED types, both full-spectrum and pure white were tested, but both proved even less visible than the RGB LEDs. Therefore, the team decided to redesign the sensor circuitry and seek out new lights before the final competition. It was also decided to utilize only the red setting of the RGB, as it was the most visible from the distance tested.

The stability test, in which each potential sensor was attached to the testing rig and towed beside a truck in clean air, returned mixed results. Though each of the designed sensors were expected to be at least somewhat stable in tow, only one sensor, designed with non-conformal fins, performed quite well. All sensors designed with conformal fins failed to nose into the wind at speeds, and all exhibited large amounts of flutter while in flight, which could have proved catastrophic to the aircraft. The sensor with non-conformal fins was able to nose into the wind and exhibited little to no flutter at our test speeds of roughly 40mph, although it continued to fly largely nose-up. This sensor with non-conformal wings was thus recommended for testing in-flight, as it far outperformed the other prototypes. Initially, wind tunnel tests had been desired, but this proved to not be feasible, as at extremely low speeds, each sensor exhibited large amounts of instability, and each proved prone to colliding with the tunnel walls, which could have resulted in damage to the sensor prototypes and the tunnel itself. The results of these tests are shown below in Table 8.1. For reference, each tail design is shown in figure 4.2.

Table 8.1: Results of Sensor Fin Aerodynamic Testing

Sensor Tail Design and Number	Qualitative Performance (1-Unacceptable, 5-High Stability)	Stability Observations
Conformal, Full-Length-of-Tail Fins (1)	2	Slightly less unstable, but still unusable. Swings significantly, but not as much as fins (2) and (3).
Conformal Stub Fins (2)	1	At every speed interval, was completely unstable, with potential to harm aircraft as it swings wildly.
Conformal Stub Fins with Ring (3)	1	At every speed interval, was completely unstable, with potential to harm aircraft as it swings wildly.
External Fins (4)	4	Best prototype performance, but still flying nose up at an angle of roughly 20 degrees. Predicted to level out more as speed increases.

Figure 8.5, shown below, shows the sensor with external tail fins in flight while attached to the testing rig. As noted, it flies straight into the wind, but significantly nose-up. It is assumed that the sensor will have a more level flight at the

higher speeds it will achieve while being towed by the aircraft, speeds we were not able to achieve in our ground tests due to space and safety reasons.

Figure 8.5: Aerodynamic stability test of sensor with non-conformal fins

Finally, the sensor deployment mechanism was tested in the lab after its construction and was found to work as designed and would be used for flight testing. This test consisted of connecting the three servos to the radio receiver and attempting to operate them with the transmitter. The results of the sensor and deployment mechanism testing phase are shown below in Table 8.2.

Table 8.2: Summary of Sensor Testing

Test	Objective	Expected Results	Actual Results
Sensor container drop test	Confirm that container protects sensor as specified in mission guidelines	Container successfully protects sensor	Container successfully protected sensor at 10”, but not at 15”
Sensor brightness test	Confirm that light pattern is visible from distance of 1000 ft. Test was conducted on a sunny day.	Light pattern visible at 1000 ft	Test failed; lights only visible at 115 ft
Sensor stability test	Test stability of sensors and select most stable sensor for flight testing	All sensors somewhat stable, sensor with non-conformal fins will be most stable	Sensor with non-conformal fins very stable, all others unstable
Sensor deployment test	Confirm that deployment mechanism deploys and retracts sensor without issue	Deployment mechanism will work as designed	Deployment mechanism worked as designed

Analysis of Sensor Drag

While the sensor used in the aerodynamic stability test conforms to the requirements of the competition, it was slightly different from the one that will be used for the competition (i.e., the final sensor body is intended to have an outer diameter of 1.5”, whereas the sensor body used for the test had an outer diameter of 1.67”). To provide useful drag estimates for Mission 3, the drag coefficient of the tested sensor was approximated using a Free Body Diagram of the sensor.

The ImageJ software [4] was used to measure the angle between the sensor tow cable and the yellow stripe along the ground in Fig. 8.5, which was used to build the Free Body Diagram in Fig 8.6.

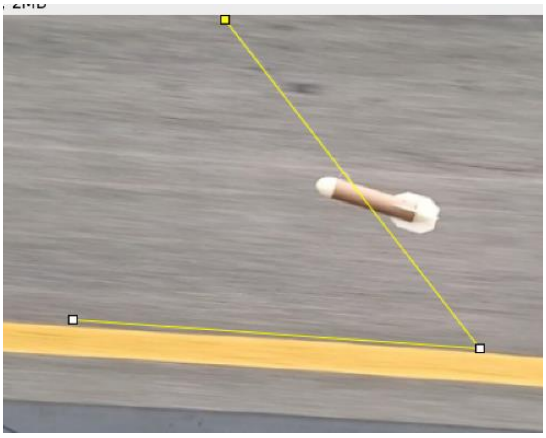

Figure 8.6: The angle measured in the ImageJ software.

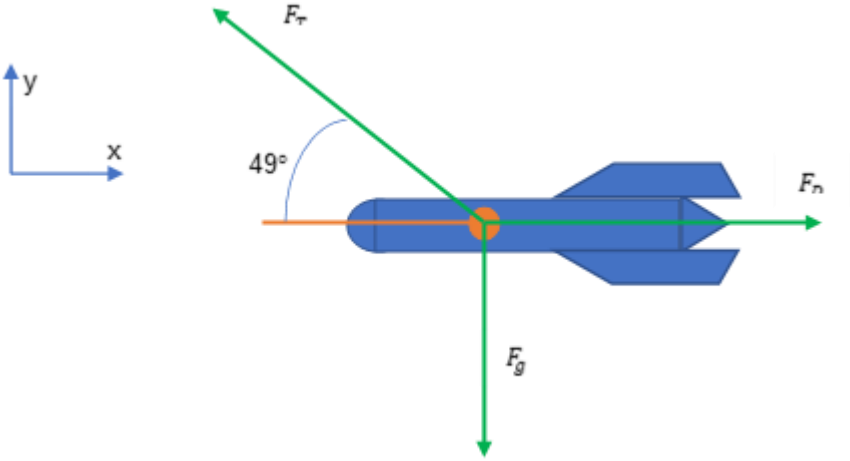

Figure 8.7: A Free Body Diagram of the sensor being towed during the aerodynamic stability test.

By balancing forces in the *x* and *y* directions and knowing the weight of the sensor (7.50 oz.) and the velocity at which it was traveling when the picture was taken (40 mph), the drag coefficient of the sensor was determined.

This required a series of simplifications. First, all forces were assumed to coincide with the center of gravity of the sensor, even though the tow cable was suspended slightly in front of the center of gravity. Secondly, the angle between the tow cable and the flight direction of the sensor was measured from an off-perpendicular point of view, so it is an approximate angle. Thirdly, the sensor did not fly parallel with the wind, meaning its frontal area was slightly larger than the area of its fuselage, but for simplicity, the frontal area was approximated as the cross-sectional area of the main body of the sensor. Combining these assumptions with weather data for the testing location (P = 28.236 in Hg and T = 40 °F) allowed for the rearranging of variables to solve for the coefficient of drag [6,7]. This drag coefficient was found to be $C_D = 6.7$.

- Flight Performance-

Figure 8.8: Photograph of prototype during taking off of first flight test

The airplane was flown at various weight configurations in an effort to determine the upper limit of wing loading. The ability to fly at high wing loading is desirable to maximize cargo without compromising stability or speed. The results of these tests were largely qualitative, based on pilot feedback of how the aircraft handled in flight. After each flight, it was decided whether to increase or decrease the weight. The results of these tests are shown in Table 8.3.

Table 8.3: Results of Wing Loading Tests			
Flight Test	**Wing Loading (oz/ft^2)**	**Pilot Comments**	**Future Design Notes**
1	38.0	- Solid pitch authority - Imprecise rolling due to coupling - Some rudder coupling - Excellent power and climb performance	- Greater wing area suggested - Add 1.25lb weight to plane for next test
2	42.6	- Feels noticeably heavier - Still short-coupled - Climb performance still excellent	- Can carry another 1.25lb for next test
3	46.7	- Feels even heavier - Acceptable climb performance - At upper end of wing-loading	- Wing loading of approximately 46 oz/ft^2 set as target for future design

In addition to wing loading tests, the maximum airspeed of the airplane was measured by flying full throttle for several seconds. The onboard data acquisition system recorded airspeeds measured with a pitot tube throughout the entire flight, which are shown in Figure 8.8. The maximum airspeed was calculated from the data and compared to the predicted value, shown in Table 8.4.

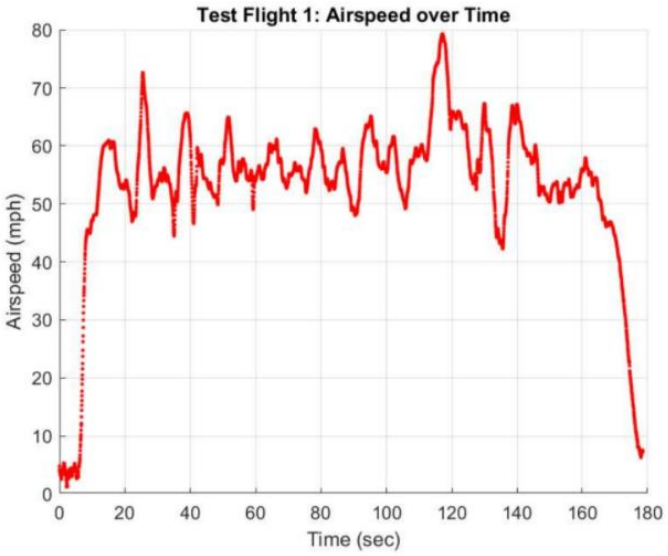

Figure 8.9: Airspeed vs Time for Test Flight 1

Table 8.4: Measured and Predicted Max Flight Speed, no weight added			
Test	Predicted Max Flight Speed (ft/s)	Actual Max Flight Speed (ft/s)	Δ%
1	123	116	-6%

The takeoff distance was also measured on the first day of flight testing. Predicted and actual takeoff distances for each flight are shown in Table 8.5 below. The large discrepancy between predicted and actual takeoff distances for the second

and third flights is due to exact procedures for takeoff not being explicitly specified. The pilot rolled onto the throttle rather than applying full throttle immediately, resulting in takeoff distances that were greater than expected.

Table 8.5: Predicted and Actual Takeoff Distances				
Test	**Weight (lb)**	**Predicted Takeoff Distance (ft)**	**Actual Takeoff Distance (ft)**	**Δ%**
1	12.1	26.5	25	-5%
2	13.3	30.5	50	+64%
3	14.6	35	50	+43%

The second day of flight testing was intended to gather more data on climb performance and max speed, along with in-flight testing of the sensor deployment mechanism. However, the prototype crashed immediately upon takeoff. The team believes that the deployment mechanism pod, which was mounted below the airplane for prototype testing, created too much drag for the plane to climb. Though data was not collected for this flight, the team learned that the previous placement of the pod external to the aircraft, even for testing purposes only, would not work. A photograph of the airplane immediately after taking off and before crashing can be seen in Figure 8.9. The final competition aircraft will have an internally mounted deployment mechanism to avoid this problem.

Figure 8.10: Photograph of airplane losing control immediately after takeoff with deployment mechanism attached.

IX. Post-Report Submission Progress

Design

a) Modifications to Report Design

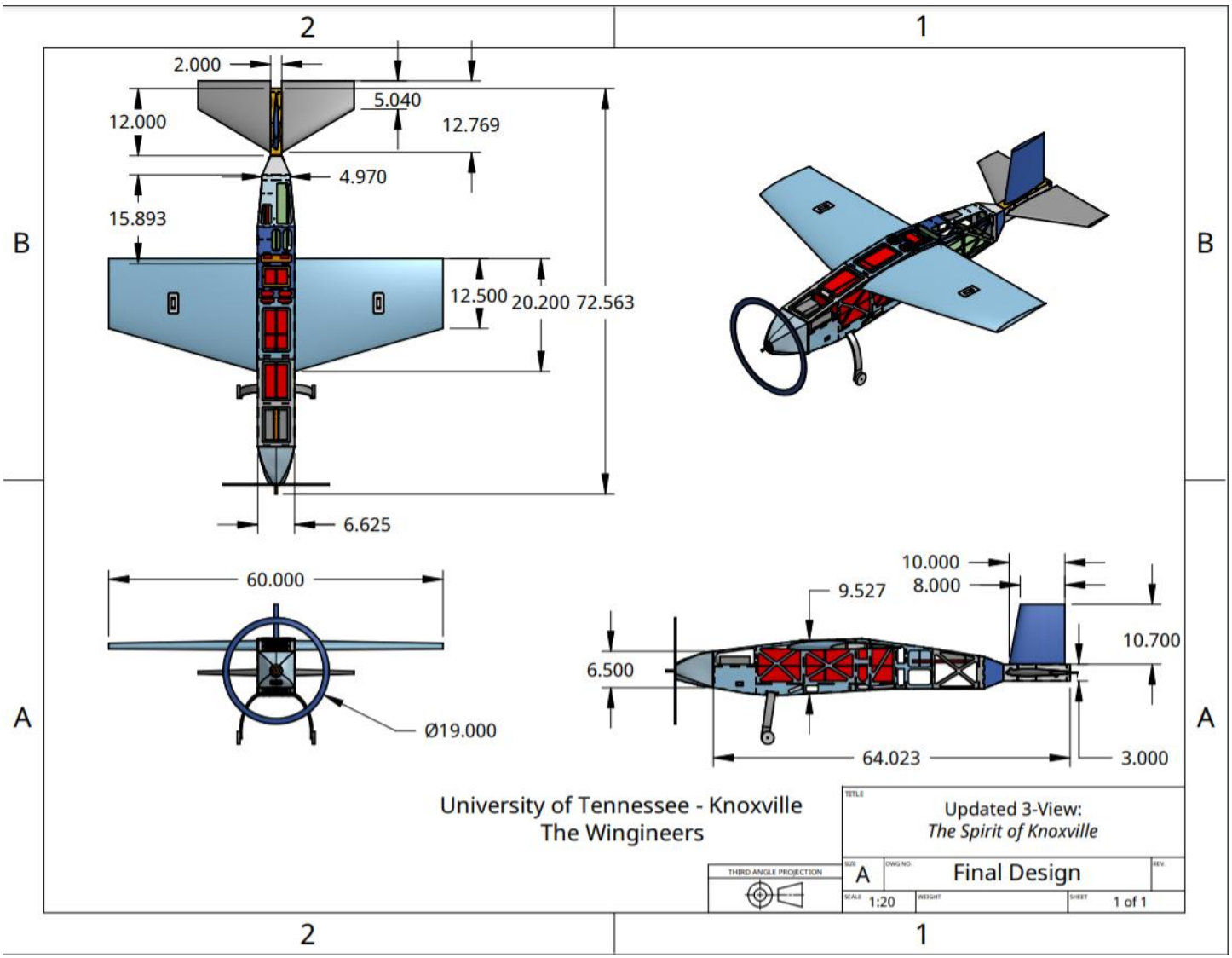

Figure 9.1: An updated drawing of the competition plane in its Mission 2 configuration. Drawn in Onshape.

After the report submission, a few minor changes were made to the design of the fuselage. First, holes were cut in the side panels for the two required electrical switches (the XT90 plug for the motor circuit and the receiver switch for the receiver circuit), and then the hole for the wing tube was raised slightly to allow sufficient clearance for the sensor simulators. The bulk of the modifications, however, occurred in the tail. In the report four-view, the fuselage panels to which the horizontal stabilizers mounted were angled inwards, but this would require that the horizontal stabilizers be cut at an angle to conform to the fuselage. This would have prevented the team from being able to control the angle of incidence, since cutting the root of the stabilizers to a certain angle would limit them to a certain angle of incidence. The team decided that a better approach would be to make this rear portion of the fuselage a rectangular prism, so that the stabilizers could be rotated to an appropriate angle of incidence before locking them into place.

The design submitted in the report contained a box for the deployment mechanism, which was based on the prototype sensor pod used in the second test flight, but this was modified in the final design to make more efficient use of the available space, as shown in Fig. 9.2.

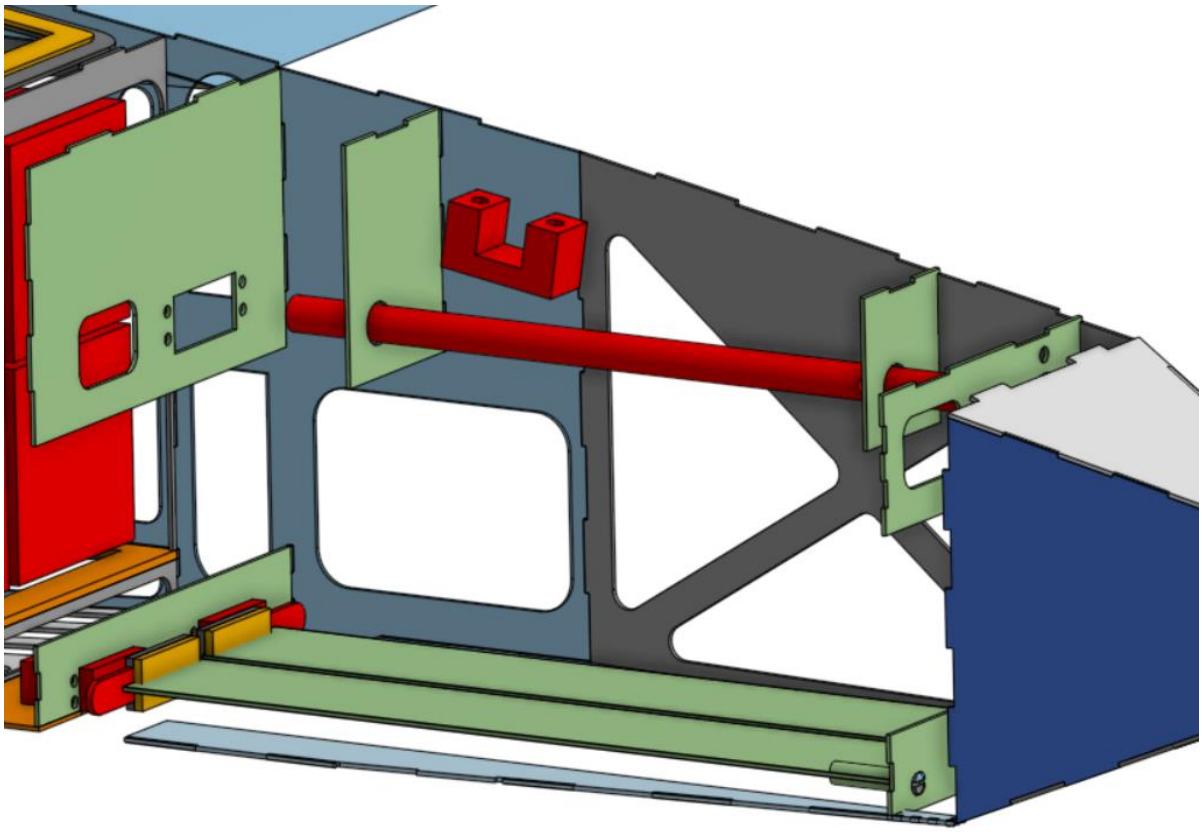

Figure 9.2: A view of the final design of the deployment mechanism, as drawn in Onshape. The ceiling and left fuselage panels are hidden.

The principle of operation remained the same: the deployment mechanism was arranged like a bomb bay, with a winch inside to retract or deploy the sensor. As with the prototype design, the deployment mechanism was designed to accommodate the deployable sensor in both of its configurations. For Mission 2, the sensor was packed inside its shipping container, which was placed on top of the bomb bay doors. While the AIAA DBF committee removed the Mission 2 flight from the competition requirements, the team still worked to ensure that the airplane would be able to perform Mission 2 as originally required. However, because the team knew that a Mission 2 flight would not be performed, some minor details were omitted for the sake of time, e.g., adding Velcro strips to the inside face of the doors to ensure that the shipping container would not move in flight.

The Mission 3 configuration was the most challenging part of the deployment system's design, since this required multiple moving parts that were robust enough to support the sensor and to avoid damage to the rest of the airplane. To complete Mission 3, the deployment system had to make a physical and electrical connection with the sensor. To ensure a firm physical connection, the weight of the sensor was supported by a braided fishing line, which was looped through a hook in the ceiling (the red U-shape in Fig. 9.2), which then wrapped around the rod, and finally was glued firmly to the rod. The electrical portion of the deployment system had to pass a PWM signal from the receiver mounted in the airplane to the Arduino microcontroller inside the sensor body, which required two wires to run from the sensor body to the receiver (i.e., a ground and signal wire). These wires were braided with the tow cable to prevent tangling during the retraction process. To complete the connection between the rotary motion of the wires around the winch to the stationary wires on the receiver side of the circuit, a slip ring was used.

b) Sensor Circuit Repair and Upgrade

There were three complete working prototypes of sensor circuits developed before the team built the most recent, reliable, and impact-resistant sensor circuit model. The first major problem of the circuit was short-circuiting. The circuit was made by soldering Arduino wires and insulating their connections with black electrical tape. Unfortunately, the tape did not adhere strongly enough due to the small area that it covered, so the tape often detached from the wires. Furthermore, the tight tolerances between the sensor body and the circuit caused the wires to twist and stretch when inserted or removed from the tube, causing some of the connections to break or short-circuit. The solution was to wrap the wires tightly with electrical tape, ensuring that the tape stuck to the wires.

The second main problem was the thinness of the electric wires. When the circuit was bent, moved, or touched, the wires would break from fatigue. Since the entire wire was cut to minimize the size of the circuit, the sensor team had to repair it with brand-new wire, which took many hours because the repair required careful and complete deconstruction and reconstruction. Moreover, the circuitry was taped with black electrical tape in every soldered part, so many times it was difficult to know where the circuit was broken, which sometimes required a complete rebuild.

The last iteration used two layers of thin balsa wood. The first piece of wood supported the two 9V batteries and the Arduino Nano. The second piece of wood supported the three 10W LEDs.

c) Final Sensor Body

The final sensor body was the same as the one described in the report. A carboard tube, 7 inches long and 1.65 inches in diameter, with 3 cutouts was used as the main body of the sensor. A nose cone and tail cone were added to this cardboard body. The nose cone was a half a prolate spheroid with a length of 1.5 inches, while the tail cone had a length of 2 inches, with 4-inch-long externally mounted fins. The fins were designed separately from the tail cone and added on as a second part to ensure that the fins were not brittle, as was the case when the part was 3D printed as a single piece.

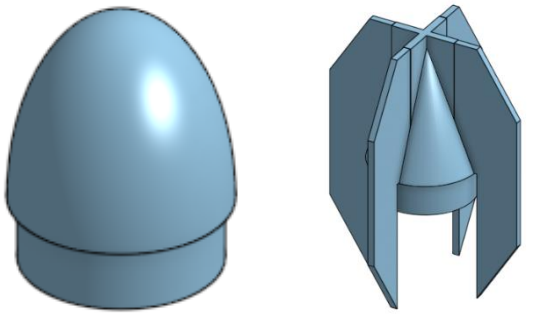

Figure 9.3: Onshape models of the nose cone and tail cone used for the final sensor design.

d) Overall Dimensions of Competition Airplane

After making the post-report submission design changes, the airplane was constructed with the dimensions shown in Table 9.1.

Table 9.1. A summary of physical dimensions of the airplane.

Dimensions of Final Airplane		
Wings	Airfoil section	NACA 2408
	Section lift coefficient	5.9086 1/rad [10]
	Wing lift coefficient (VLM)	3.718 1/rad
	Reference Area	6.722 ft^2
	Root chord (fuselage centerline)	20 in.
	Tip chord	12 in.
	Span	60.5 in.
	Aileron area	.75 ft^2 (11.15% S_{wing})
	Taper Ratio	0.6
Horizontal Stabilizers	Airfoil section	NACA 0010
	Area	1.66 ft^2
	Root chord (fuselage centerline)	13 in
	Tip chord	4.75 in.
	Span (tip-to-tip)	27 in.
	Elevator area	.3403 ft^2 (20.5% $S_{h\text{-}stab}$)
	Aspect ratio	3.05
	Leading edge sweep angle	31.4°
Vertical Stabilizer	Airfoil section	NACA 0012
	Area	.6905 ft^2
	Root chord (fuselage centerline)	10.5 in
	Tip chord	8 in
	Span	10.75 in
	Rudder area	.21875 ft^2 (31.68% $S_{V\text{-}stab}$)

Construction

a) Raw Materials

Figure 9.4: Main materials used for construction, LitePly Plywood (left) and insulation foam (right).

b) Summary of Construction Process

- **Wings:** For the final iteration of the airplane, a foam core wing construction with a balsa skin was selected. First, plywood was glued to each side of two 2'x4'x2" sections of pink insulation foam. Then, using laser-cut plywood guides, the core of the wing was cut into the correct airfoil shape. Using a 3D printed guide, a hole for the phenolic section of the wing tube was then cut out of each wing.

Figure 9.5: Foam core cut into the correct shape by the hotwire cutter and phenolic tube installed into the core.

Next, strips of 1/16 inch balsa were laid out and taped into a sheet. Epoxy was applied to one side of this sheet and this sheet was then placed over the foam core. This was then placed back into the wing beds and weighted overnight to form the skin of the wing into the correct airfoil shape.

Figure 9.6: Skinning process for foam core wings.

The surface of the wing was then sanded smooth, and the root and tip caps were added to both wings.

Figure 9.7: Components along the inside of the root cap including alignment pins and locking bolt for the wing screw.

The trailing and leading edges were cut from the wing and replaced with balsa. This balsa was then sanded to the correct shape. The aileron was then cut out of each wing, and balsa caps were added to the area where the hinges mounted the ailerons to the wings, both on the wing and aileron itself. This was sanded to an angle and hinges were installed into the wing bed. Plywood support was added on the aileron where the control horn is mounted, and the aileron was then hinged onto the wings.

Figure 9.8: Balsa supports along the hinge line between the wing and aileron, showing the hinging for the aileron and the support area for control horn.

Next, a 3D printed servo bay was installed into the wing with epoxy. The wings and control surfaces were then sprayed with 3M adhesive spray and laminate was ironed onto the wings. Finally, servos, control horns, and control rods were added to the wings.

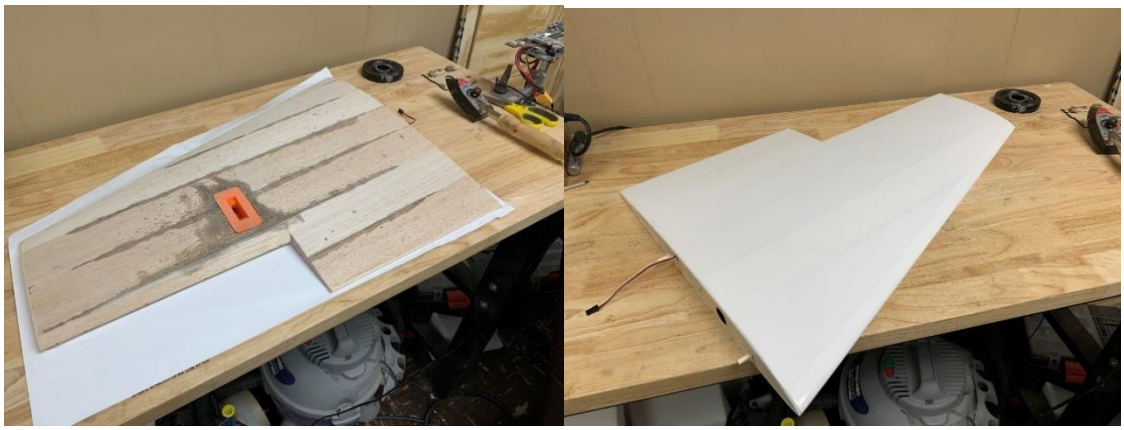

Figure 9.9: Installation of the servo bays into the wing and covering of completed wing.

- **Stabilizers:** For the final iteration of the airplane, EPP foam was chosen as the construction material. Firstly, foam cores were cut to the correct dimensions, and then laser-cut plywood guides were used to hotwire cut the airfoil out of these foam cores, similar to the process done for the wings. The stabilizers were then sanded smooth, and a channel for the phenolic tube was cut out with the hotwire cutter. The phenolic tube was glued in with Goop adhesive, along with 4 carbon fiber spars in each of the stabilizers. This was allowed to dry in weighted wing beds, and then a hole for the elevator servo was cut in each of the stabilizers. The stabilizer leading and trailing edge was sanded to the correct shape, and plywood was installed around the servo bay to add structural support to this area. A balsa control surface was sanded to the correct shape, and the entire stabilizer and control surface was sprayed with 3M adhesive spray. The stabilizer was then covered with laminate, and the control surfaces were hinged on using this laminate. Finally, servos, control horns, and control rods were added to the stabilizers, along with a root cap. The stabilizers were then mounted to the fuselage using a carbon fiber tube as well as wood screws through the root cap of the wing.

- **Fuselage:** The fuselage was constructed using a laser-cut lite plywood method. First, the structure of the fuselage and all related components were designed in Onshape, with joints designed to make the physical assembly as robust as possible. Then, the pieces of the fuselage were exported as .dxf files and put into 4'x8' sheets. These sheets were cut on a laser cutter using 1/16 inch and 1/8-inch plywood, depending on the specifications of each part. These pieces were then sanded to remove any excess material that may not have been removed by laser cutting, and dry fit together into the fuselage shape. Once it was confirmed that all pieces fit together well, the fuselage was then glued together using wood glue, with a level and speed squares to ensure that the fuselage was as true to the CAD model as possible. Epoxy was then added in areas that needed reinforcement, such as the landing gear mount, the motor box, and the deployment system area. Next, the entire outside of the fuselage was sanded smooth, extension wires were added leading from the tail to the receiver mounting area, and the fuselage was covered in MonoKote. Finally, the remaining electronics (flight controller, electronic speed controller, motor, and receivers) were added to the plane, and the landing gear, vertical and horizontal stabilizers, and wing were attached to the completed fuselage. The control surfaces were then trimmed and calibrated to ensure proper functionality.

Figure 9.10: Laser Cut Panels

Figure 9.11: Deployment System Construction

Figure 9.12: Drying of Fuselage after Applying Wood Glue

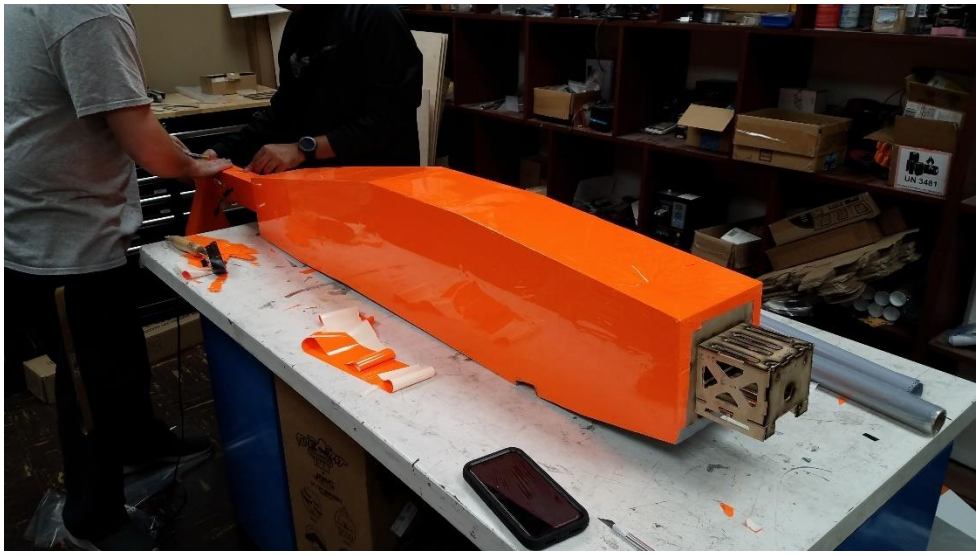

Figure 9.13: Covering the Fuselage with MonoKote

Flight

a) Pre-flight Testing

- Deployment System Testing

Since the previous flight test ended before the prototype deployment system could be tested, the deployment system in the competition plane had not been proven in flight prior to Flight Test 3. Thus, a series of ground tests were performed to ensure that the deployment system and sensor would behave as expected in the air.

First, the operation of the two door servos was verified by connecting them to a receiver, which was paired with the transmitter that would be used for the flight test. While the servos had 120° of motion, it was necessary to ensure that the servo horns were mounted onto the servo shafts such that their range of motion would correspond to the desired range of motion (i.e., so that the doors would open and close). The orientation of the servo horns was adjusted as needed. Then, the physical connections for the winch were tested by rotating the continuous servo forward and backward, and then holding it at its neutral setting. This was done to calibrate the transmitter settings (i.e., to set the PWM frequency at which the servo would be full-speed forward, full-speed backward, and motionless).

The electrical portion of the winch was tested as well. First, the operation of the sensor circuit was verified with a separate receiver, and then the sensor was connected to the signal and ground wires in the deployment system. The PWM frequency corresponding to the “lights-on” setting was sent from the transmitter to the receiver, and the lights were verified to turn on and off on command. This verified that the signal did not degrade between the receiver and the Arduino Nano, despite the low voltage of the signal, the contact resistance from the soldered wire connections, and the length of cable through which the signal traveled.

Because the forces generated by the rudder and elevators would be transmitted to the rest of the airplane through the structure of the deployment system, it was important to ensure that the structure was adequately reinforced prior to flight. To highlight areas that may require additional reinforcement, the tow cable was fed through the hook in the ceiling and slowly pulled; the portions of the ceiling that moved significantly were reinforced with tongue depressors or scrap pieces of wood.

The behavior of the system in flight was simulated as closely as possible. In flight, the tension acting through the tow cable would be the resultant of the sensor's weight and drag, so to simulate the real tension, the sensor drag force calculations from Section VIII were used, and weights were added to the sensor body to represent this drag force. This simulated the stress that was estimated to act on the winch in flight. Despite this extra load, the winch operated successfully.

Finally, the entire deployment process was performed on the ground (without the bulk of the extra weights to simulate the drag force). The sensor was connected to the tow cable and to the signal and ground wires, spooled up into the fuselage, and the doors were closed. Then, the doors were opened, the sensor was deployed halfway to the ground, the lights were turned on, and then the process was reversed. This process revealed the need to connect the three cables firmly together; the slack in the electrical wires would occasionally wrap around the winch rod, opposite to the direction in which the wires were intended to spool, which prevented the sensor from deploying. To solve this problem, the wires were zip-tied together, and these zip ties were glued to the wires to ensure that there would be no slip.

- Propulsion and Controls Testing

The propulsion system used in the final airplane was the same one used in the prototype, so it was tested before Flight Test 3 to ensure that it was undamaged by the crash at the end of Flight Test 2. The propulsion circuit was set up and assembled (except the propeller) and throttled up, verifying that the propulsion system was undamaged by the crash. In addition to the throttle control, the aileron, elevator, and rudder controls were tested with the transmitter to ensure that they moved as expected.

b) Performance Characteristics

Table 9.2. A summary of the performance characteristics of the airplane.

Performance Characteristics of Final Airplane	
Parameter	**Value**
Wing loading	
Mission 1	34.58 oz/ft^2
Mission 2	45.71 oz/ft^2
Mission 3	34.42 oz/ft^2
Location of CG (from firewall)	
Mission 1	19.17 in
Mission 2	19.25 in
Mission 3	19.17 in
Location of NP (from firewall)	
Mission 1	20.8 in
Mission 2	20.8 in
Mission 3	20.8 in
Static Margin (see Appendix A for calculations)	
Mission 1	8.5 %
Mission 2	8 %
Mission 3	8.5 %
Est. Takeoff Distance	
Mission 1	32.77 ft
Mission 2	52.87 ft
Mission 3	62.48 ft
Actual Takeoff Distance*	
Mission 1	50 ft
Mission 2	------
Mission 3	45 ft
Duration of Flight	
Flight Test 3.1	4:04
Flight Test 3.2	3:19
Voltage Drop per battery pack	
Flight Test 3.1	1.3 V
Flight Test 3.2	1.1 V
Est. Cruise Speed	122 ft/s (83.2 mph)

*Note: Pilot rolled onto throttle and was not attempting to take off in minimum distance.

c) Results from Flight Test 3

Flight Test 3 served as our official flight for the competition, as all footage for the video submission was captured during this test. It consisted of two flights: one with no payload (sensor weight was simulated with lead shot), where the objective was simply to successfully takeoff, fly long enough for in-flight footage, and land successfully, and a second with the sensor payload, where the objective was to capture footage of the sensor deploying, stabilizing in flight, and retracting back into the plane. Both flights were successful with footage from team members captured at approximately 25', 50', 75', and 100', as well as a GoPro camera at the beginning of the runway and a FPV drone capturing overhead footage. Besides video footage, the only other data collected was pilot feedback. According to Sam Pankratz, the design's pilot, the plane had crisp roll authority with a substantial amount of excess power, making it a quick plane and relatively easy to control. The takeoff of the first flight was rough since the ailerons had never been trimmed in flight, but once trimmed, the flight characteristics were easily predictable. One thing that was noted was that the plane lacked some in elevator authority. The

pilot noted that this could likely be fixed by changing the geometry of the fuselage to allow more of the elevator to be out of the downwash of the fuselage. During the second flight, the deployment system and sensor both performed as expected, with the sensor deploying in flight in approximately 20-30 seconds, remaining stable in flight and successfully lighting up in the predetermined LED pattern, and then retracted back into the plane in approximately 30 seconds. One issue that was noted was that, during retraction, the sensor began to become unstable when it reached the downwash of the propellor. But given that the airplane had a single engine, this was unpreventable unless the deployment system was mounted away from the fuselage centerline.

Overall, since all main objectives were met during Flight Test 3, most improvements to the design involve increasing the speed and payload capacity of the airplane. The geometry of the fuselage could possibly be reworked to allow for more elevator authority, and possibly also reduce the component weight and cross-sectional area of the fuselage where possible. For the other components of the design, efforts could be made to reduce the overall empty weight of the aircraft through speed holes, more careful construction to minimize adhesives and supports, and by swapping out any denser materials with possible lighter variants (using a more lightweight filament for 3D printed parts, manufacturing a lighter landing gear, etc.).

d) Gross weight and component weights

Table 9.3. A summary of the airplane weight in each mission configuration, as well as a list of component weights.

Component	Mission 1 Weight (lb)	Mission 2 Weight (lb)	Mission 3 Weight (lb)
Fuselage (incl. tail, landing gear, deploy. sys., and wiring)	6.950	6.950	6.950
Receivers and Flight Controller	0.051	0.051	0.051
Motor	1.345	1.345	1.345
Batteries	1.508 3.016 (total)	1.508 3.016 (total)	1.508 3.016 (total)
ESC	0.328	0.328	0.328
Wings	2.940	2.940	2.940
Tail ballast	0.500	- -	- -
Sensor simulators	- -	0.55 each (4.4 for 8)	- -
Deployable sensor	- -	0.440	0.440
Deployable sensor container	- -	0.095	- -
Overall	**15.13**	**20**	**15.06**

X. Bibliography

[1] University of Tennessee, Knoxville Design, Build, Fly Team, “2020-21 Design, Build, Fly Proposal”, October 2020.

[2] MATLAB, Software Package, Ver. R2020a, MathWorks, Natick, MA, 2020.

[3] Loftin, Laurence K, Jr., and Cohen, Kenneth S., “Aerodynamic Characteristics of a Number of Modified NACA Four-digit-series Airfoil Sections,” NACA-TN-1591, June 1948.

[4] Rasband, Wayne and contributors. ImageJ. Public Domain software. National Institutes of Health. http://imagej.nih.gov/ij.

[5] “1000 Forts Pound Berlin,” Archival Footage, British Pathé, Reuters, retrieved 19 February 2021. https://www.britishpathe.com/video/1000-forts-pound-berlin/query/1000+FORTS+POUND+BERLIN

[6] “(KDKX) Knoxville Downtown Island Airport,” Aircraft Owners and Pilots Association, retrieved 18 February 2021. https://www.aopa.org/destinations/airports/KDKX/details.

[7] “Alcoa, TN Weather History / McGhee Tyson Airport Station,” Weather Underground, retrieved 18 February 2021. https://www.wunderground.com/history/daily/KTYS/date/2021-2-12.

[8] Raymer, Daniel, “Aircraft Design: A Conceptual Approach,” American Institute of Aeronautics & Aerospace, 1 August 2012.

[9] Bond, Robert. AE 370 Course Notes. Unpublished.

[10] **“**NACA 2408” NACA 2408 airfoil, Airfoil Tools, retrieved 1 February 2021. http://airfoiltools.com/airfoil/details?airfoil=naca2408-il

[11] Onshape, Software Package, Ver. 1.127.26944.884b966bfb3d, Present, Onshape Inc., Boston, MA, 2013.

[12] Bond, Robert. AE 422 Course Notes. Unpublished.

[13] Loth, Eric. “Lecture 4: Aerodynamics.” Aerospace Engineering 440 A/C Lecture.” September 2009. SlidePlayer.com Inc. https://slideplayer.com/slide/8573460/

Appendix A: Static Margin Calculations

To calculate the static margin for each mission configuration, Eq. A.1 was used:

$$margin = \frac{|CG - NP|}{CG} * 100\% \quad (1)$$

where *CG* represented the distance from the firewall to the center of gravity and *NP* represented the distance from the firewall to the neutral point of the airplane. To determine the static margin for each configuration, the first step was to determine the location of the center of gravity. This was done by balancing the airplane on a pole, supporting it from different points until the airplane appeared not to pitch. The distance from the firewall to the center of the pole was recorded as the location of the center of gravity.

The second step was to determine the neutral point of the airplane. This was the same in all configurations, since the wings, tail, and the distance between them were constant for all three missions. The process for this calculation was taken from [9], beginning with Eq. A.2:

$$h_n = \frac{h_{nw} + h_l \eta_t \left(\frac{S_t}{S}\right)\left(\frac{a_t}{a}\right)(1-\varepsilon_\alpha)}{1 + \eta_t \left(\frac{S_t}{S}\right)\left(\frac{a_t}{a}\right)(1-\varepsilon_\alpha)} \quad (2)$$

The distance from the firewall to the quarter-chord of the wing (at the centerline of the fuselage) was measured and used as $(h_{nw} * c_{mac})$. To isolate h_{nw}, the mean aerodynamic chord was calculated with Eq. A.3 [9]:

$$c_{mac} = \frac{2}{3} * c_r * \left(\frac{1+\lambda+\lambda^2}{1+\lambda}\right) \quad (3)$$

The mean aerodynamic chord was found to be 16.3”. The next step was to determine the lift curve slopes for the tail and the wings, which was done using the vortex lattice method [12]. To be conservative, the tail efficiency was taken as 0.9. To determine the slope of the downwash angle vs. angle of attack curve, two plots were used, according to the process from [9]:

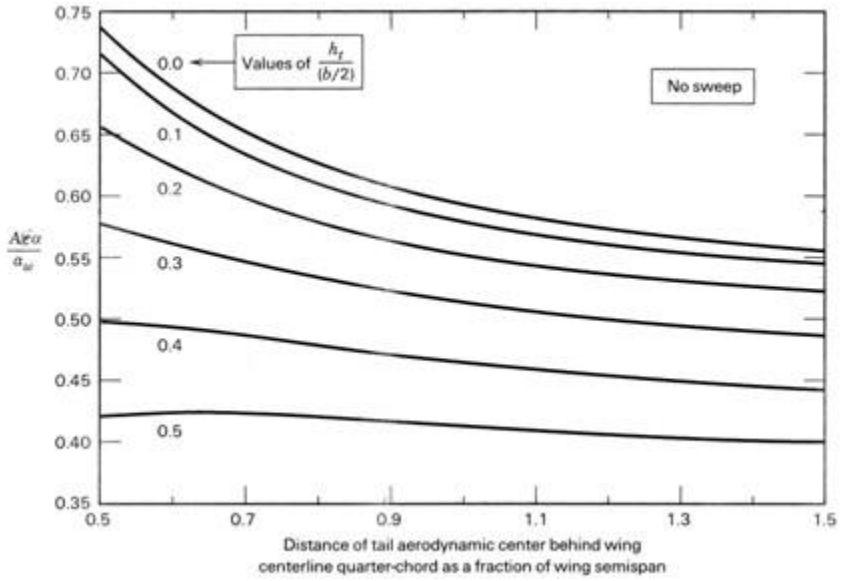

Figure A.1. The plot used to determine ε_α without sweep (from [13], who adapted it from McCormick).

To use this plot, the vertical separation between the aerodynamic center of the wings and the aerodynamic center of the tail had to be known. This was measured as h_t = 6”. Thus, the curve corresponding to $\frac{h_t}{\left(\frac{b}{2}\right)} = \frac{6"}{(60.5"/2)} = 0.198 \approx 0.2$ was used. The value along the horizontal axis was determined using the measurements recorded for the location of the aerodynamic center of the wing and the aerodynamic center of the tail. The distance between these two points (along the

fuselage centerline) was measured to be 37.5", so as a fraction of the wing semispan, this value was $\frac{37.5"}{(60.5" / 2)}$ = 1.24. For the 0.2 curve at 1.24 along the horizontal axis, $\frac{AR*\varepsilon_\alpha}{a_w}$ = 0.55. Knowing the aspect ratio of the wing and the slope of the lift curve for the wing (from the vortex lattice method; listed in Table A.1), ε_α could be determined. Note that this was the slope of the downwash vs. angle of attack curve for the case of no wing sweep. To correct this value for the case of nonzero wing sweep, a second plot was needed (Fig. A.2).

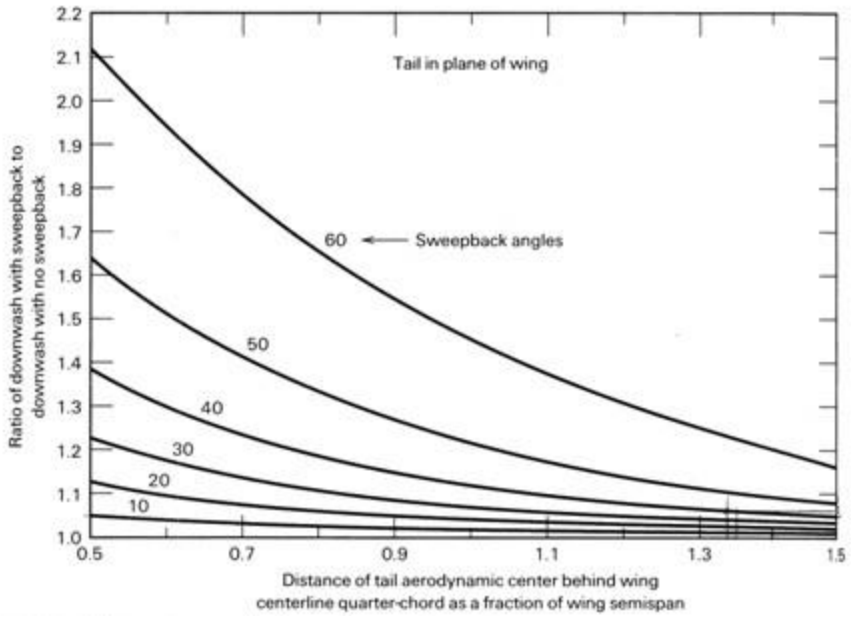

Figure A.2. The plot used to determine ε_α with sweep (from [13], who adapted it from McCormick).

As before, the value along the horizontal axis was 1.24, and the sweep angle for the tail at the leading edge was determined to be 31.4°, so the value along the vertical axis was 1.05, meaning $\frac{\varepsilon_\alpha(sweep)}{\varepsilon_\alpha(no\ sweep)}$ = 1.05, or $\varepsilon_\alpha = 1.05 * 0.55 * \frac{a_w}{AR} = 0.5775 * \frac{3.718\frac{1}{rad}}{3.75} = 0.573\ 1/rad$. The values substituted into Eq. A.2 are summarized in Table A.1.

Table A.1. A summary of inputs for the neutral point calculation.

Variable	Value
h_{nw}	1.1196
h_l	3.4202
η_t	0.9
S_t	229.5 in^2
S	960 in^2
a_t	3.312 1/rad
a	3.718 1/rad
ε_α	0.573

This yielded h_n = 1.276. Thus, the location of the neutral point was a distance of h_n*c_{mac} = (1.276)*(16.3") = 20.8" behind the firewall. Following Eq. A.1, this meant a static margin of 8.5% for Missions 1 and 3 and 8% for Mission 2.

Appendix B: Capstone Reflection

This project took quite a bit of time and effort but was ultimately rewarding. Other senior design projects were purely design projects, never reaching the point of physically constructing the design, but ours involved a very hands-on construction stage. In this sense, it was one of the more fulfilling projects; at the end, we all got to see our airplane fly. This construction process, however, was often a significant source of stress, particularly with the pandemic; because our project involved physical construction, we had to spend time physically working so when anyone went into quarantine, the schedule had to be adjusted. As the team lead, it was my job to address these issues; I divided the labor so that we could get done what we needed to get done, but I had to rearrange this division of labor more than once. This was just an unavoidable part of the pandemic; like everyone, we came up with a good plan, and then we had to come up with another good plan. And then another.

Another challenge was my inexperience with remote-controlled airplanes. I knew the basics of airplane performance but had never worked with hobby-scale airplanes before, and certainly had never constructed one from scratch. This was a steep learning curve, to say the least. As the team lead, I was responsible for helping to keep the team on track, which meant I had to know at least generally what everyone was working on. Partially by asking those who knew far more than I, and partially by teaching myself, I learned many things about airplane electronics and controls (how radio receivers and transmitters work, how the signal is carried from the receiver to the motors, etc.) and structural assembly (how to ensure that the structure is firm but not too heavy, etc.).

I have been fortunate, however, to have a good team with whom to work. Everyone has contributed, and one of our team members has worked with remote-controlled airplanes extensively, so he was a valuable resource. This experience gave me a certain confidence in my ability to be an engineer after graduate school. By building the airplane from scratch, I learned what it looks like to go from a general design concept to a specific design, and from the design to a physical product. This project was hard because we had to design and manufacture every single part of the airplane (except the vertical stabilizer; we borrowed that from last year's airplane), but this also made it a very insightful project. Had we stuck with a design, rather than designing, constructing, and flying the airplane, we probably would have lost sight of what we were doing. In the design world, it's easy to say things like "this servo motor will be attached to this rod somehow," but when this has to be assembled physically, these details must be considered. I therefore learned more about servo motors by working with them physically than I would have if they were just features of our design. It was really cool to have the black box opened and see how the mechanics of remote-controlled airplanes work, because this practical experience is not something that is often taught in the classroom.

It's easy to write off the difficulty of this experience as simply the result of inexperience with airplane construction, but I've realized that this is often the case in engineering; engineers do not have a prescribed manual for solving everything, so the ability to teach oneself new things and to work on a team is important.

In addition to the many engineering lessons I've learned, I learned a fair amount about working on a team. Engineering often requires completely new solutions, but often these solutions are hybrids of solutions to other problems, so it is very helpful for an entire team of people with diverse backgrounds to work on the problem. The solution that one person would have developed may be far less efficient or robust than one developed by someone else with a different set of experiences. Engineering works best without pride; to work on a team of people to solve a problem, one must recognize that other people with different experiences may be able to come up with a better solution. In the context of my senior design, this meant listening to every idea and going with the one that seemed best to the team as a whole, not just to one person. Sometimes an executive decision was necessary, but generally we worked to avoid making one-sided decisions.

Overall, however, I'm relieved that the airplane flew. There were, admittedly, several unknowns; even after making and learning from the first prototype, there were several aspects of the final airplane that hadn't been tested, like the behavior of the sensor deployment system in flight. It was rewarding to watch the chase drone footage after the final flight test and to reflect on each of the details that went into the airplane. I remember picking up from the store the insulation foam that became the wings, glittering in the afternoon Tennessee sun. I remember spending many hours looking at the deployment system design, wondering how I could prevent all of the unknowns from damaging the airplane, but it behaved wonderfully. But in the end, all of this work paid off. They say that any airplane can land, but only the good ones can take off again, and I am proud to say that ours falls into the second category.